Master's Thesis

Characterization for enhanced mechanical properties and energy storage performance of tin oxide nanorods-carbon fiber composites

OBum Kwon

Department of Mechanical Engineering

Graduate School of UNIST

2017

Characterization for enhanced mechanical properties and energy storage performance of tin oxide nanorods-carbon fiber composites

OBum Kwon

Mechanical Engineering
Graduate School of UNIST

Characterization for enhanced mechanical properties and energy storage performance of tin oxide nanorods-carbon fiber composites

A thesis
submitted to the Graduate School of UNIST
in partial fulfillment of the
requirements for the degree of
Master of Science

OBum Kwon

11. 29. 2016
Approved by

Advisor
Hyung Wook Park

Characterization for enhanced mechanical properties and energy storage performance of tin oxide nanorods-carbon fiber composites

OBum Kwon

This certifies that the thesis of OBum Kwon is approved

11. 29. 2016

Hyung Wook Park

Young-Bin Park

Han Gi Chae

Summary

The use of multifunctional materials is ever increasing day by days. Multifunctional materials contain structural and non-structural functions and could improve system performances through reducing weight and volume of the system. Especially, carbon fiber reinforced composites are regarded as one of the outstanding multifunctional materials which can offer structural and electrochemical energy storage functions.

Performances of carbon fiber composites are critically determined by interphase interactions between fibers and matrix. Therefore, many surface treatment methods are utilized to improve composite properties. Among the surface treatments, the whiskerization method does not degrade the carbon fiber properties via nanostructure deposition. Therefore, the tin oxide nanorods were synthesized on woven carbon fiber (WCF) surface using two step hydrothermal methods as a sort of whiskerization treatment. The SnO_2 nanomaterials are widely used as energy storage devices owing to its wide band gap and high excitation energy as a semiconductor material. Therefore, the mechanical and electrochemical performances of tin oxide nanostructured carbon fiber composites were studied.

In this thesis, the mechanical and electrochemical energy storage performances were characterized via tin oxide nanorods on carbon fiber surface. The tin oxide nanorods were synthesized using hydrothermal method and utilized as secondary reinforcements in composite. X-ray diffraction (XRD), scanning electron microscopy (SEM), X-ray photoelectron spectroscopy (XPS), and Brunauer-Emmett-Teller (BET) method were used for observing morphology and structure of tin oxide nanorods arrays.

The improved mechanical properties of the impact absorbed energy (71.65%), ultimate tensile strength (35.07%), in-plane shear strength (49.07%) and elastic modulus (44.15%) were obtained for 70 mM of SnO_2-carbon fiber composite.

The structural composite capacitors were fabricated with two layers of SnO_2-carbon fiber electrodes, one layer of glass fiber separator and multifunctional polymer electrolyte. The electrochemical energy storage performances were characterized by cyclic voltammetry, galvanostatic charge-discharge and electrochemical impedance spectroscopy. Multifunctional structural capacitors were achieved 147.53 mF/g of specific capacitance, 15.06 mWh/kg of energy density, and 1.16 W/kg of power density for 30 mM of SnO_2-WCF composite capacitor

The SnO_2 nanostructures were grown by self-assembly mechanism under high pH of about 13. The growth of SnO_2 was enhanced mechanical and electrochemical energy storage performances than conventional carbon fiber composites.

Contents

LIST OF FIGURES

LIST OF TABLES

1. Introduction

1.1. Carbon fiber reinforced composites

Carbon fiber reinforced composites (CFRPs) are widely utilized in industries where low weight and high strength are required, for instance, CFRPs are used in aircraft parts due to their abilities to reduce fuel consumption and enhance overall system efficiency. Their high specific strength and stiffness enable the high mechanical performance at a reduced weight. The fatigue tolerance, chemical and corrosion resistance of CFRPs make them desirable for high-tech structural engineering applications [1]. Therefore, it has been considered as an ideal material for aerospace industry which requires reduced weight and increased performance. However, the superior properties of CFRP are critically controlled by interphase status between fibers and matrix. Carbon fibers without surface treatment depict low interlaminar shear strength (ILSS) due to the chemically inert surface. The weak adhesion and poor bonding between fibers and matrix are the key reasons of low ILSS. Thus all carbon fibers are used with surface treatments [2]. These treatments enhance the surface functional groups and surface area and thus improve interphase bonding within interphase region [3, 4]. Surface treatments can be classified into oxidative and non-oxidative treatments. Oxidative treatments are carried out chemically [5] or electrochemically [6] via gas- or liquid-phase oxidation. The non-oxidative treatments are performed through deposition of more active materials such as highly effective whiskerization [7] or plasma treated to enhance interlaminar bonding.

The whiskerization is considered as a promising treatment which enhances interphase interactions without chemically deteriorating fiber surface [2, 8]. Whiskerization method, the deposition of an array of nanostructures (whiskers) on the fiber surface, allows the enhancement of the interphase properties via fiber interlocking and thus alleviates stress concentration at interlaminar region with reinforced interphase formation. Many carbon based whiskers, such as carbon nanotubes (CNTs), graphene oxides (GOs), and other fillers, are extensively used to improve the performances of CFRPs, however, the properties have not been enhanced to the desirable level. In order to be a successful reinforcement material, the filler should have a large aspect ratio, good alignment, and uniform distribution in the matrix [9]. One-dimensional (1D) metal oxide nanomaterials are widely explored as a sort of whisker due to its wide applications in sensors and electric devices [10].

1.2. Tin oxide nanomaterials as secondary reinforcement

Among the metal oxide nano-materials, tin oxide (SnO_2) has been extensively utilized in many researches, for instance, gas sensors [11], transparent electrodes [12], solar cells [13] and supercapacitors [14] owing to the wide band gap (E_g = 3.6 eV, at 300K), large excitation binding energy (130 meV), high thermal shock resistance [15] and high theoretical capacitance (782 mAh/g) [16].

Several synthesis methods of tin oxide nano-materials such as sol-gel [17], chemical vapor deposition [18], thermal evaporation[19], solvothermal[20], and hydrothermal techniques[21] have been reported. Among the different methods, the hydrothermal process has been the most favorable because it is cost effective and environmentally safe, lowers energy consumption. Synthesis of SnO_2 1D nanorods (NRs) on carbon fiber surface as secondary reinforcements in CFRPs has yet to be reported while several hydrothermal synthesis techniques for SnO_2 nanostructures have been reported [21-24].

1.3. Structural composite capacitor as multifunctional material

There have been enormous interests in developing multifunctional materials that simultaneously present structural and non-structural functions. Multifunctional materials exhibit load-bearing structural capability with at least one of additional function such as electrical, thermal, optical, chemical and electromagnetic properties [25], and thus can achieve the improvement of system performance via reducing the redundancy (weight and volume) of the system. The ordinary composites are made from two or more different materials which contain physically or chemically disparate properties, but when combined, it produces improved engineering performance than individual components [26]. Therefore, the composite materials are ideally suited for constructing multifunctional materials which can fulfill more than one goal within a system.

The combination of structural and electrochemical energy storage functions is one example of multifunctional material and has great potential in aerospace, electric automobile, and portable electronic applications [27, 28]. It is challenging to develop multifunctional composite materials which can perform superior performance in structural and energy storage functions simultaneously. Several papers have reported multifunctional structural capacitors using carbon fibers electrodes have been chemically activated [29], sized via carbon nanotube [30] and deposited with monolithic carbon aerogels [31]. However, tin oxide nanostructured carbon fiber based structural capacitors have not yet been published.

1.4. Research motivation and objectives

This thesis work was motivated by a realization that the carbon fibers are utilized both for structural composites (CFRPs) and electrochemical energy storage devices, and hence, both CFRPs and electrochemical devices are generally assembled in a laminated form. Combining structural and energy storage functions is a considerable challenge, since the structural and non-structural functions are usually conflicting. However, the rewards of developing these optimum materials are huge and thus such materials enable the significant savings in system level mass and volume [32].

The superior mechanical properties of CFRPs are crucially controlled by interphase state between fiber surface and matrix. Therefore, enhancing the interlaminar interaction is essential for the successful development of composite material. Whiskerization is one of effective methods to reinforce interphase bonding via creating an interconnected network embedded in composites. The entangled interphase networks by whiskers, such as metal oxide nanostructures, increase the interactions between fiber surface and matrix and thus enhance the overall mechanical properties. When material loads are exerted on the composites, they absorb its energy and deform concurrently. During deformation, the cracks are caused by the applied load and propagate to the interface region. This progressed crack incurs the delamination in the interlaminar layer between fibers and matrix which is representative reason of mechanical property degradation. Entangled interphase network by nanostructures could hinder crack propagation as kind of obstacles and thus increases the resistance to external loads. Therefore, the metal oxide nanostructures at carbon fiber surface, reduces stress concentrations and enhances the load transfer within interlaminar region as secondary reinforcement of composite material. In this work, the tin oxide nanorods are focused among the metal oxide materials.

In this work, tin oxide nanorods are focused among the metal oxide materials. ZnO and CuO are also extensively facilitated as whiskerization materials in carbon fiber reinforced composites [33, 34]. ZnO nanostructures are enormously investigated for their piezoelectric and semiconductor properites. Owing to the large band gap (3.4 eV) and large excitation energy (63.1 meV), ZnO nanowires are interested to many research fields such as strain sensing, acustic sensing, and energy harvesting [35-37]. In addition, ZnO nanostructures can be synthesized at low temperature (<90℃) in aqueous solution, therefore; those are frequently used as secondary reinforcements for enhancing mechanical proeperties of composite materials. On the other hand, CuO nanosturcutres are also facilitated as whiskers for enhancing interfacial networks. CuO is utilized as p-type semiconductor materials beacause of narrow band gap of 1.2 eV [38]. CuO nanostructures are interested in several application

areas such as field emitters, rectifiers, and storage devices [39-41]. In addition, this nanomaterial is well known with regard to their high temperature superconductivity and relatively large magnetoresistance [42, 43]. CuO is considered as starting growth materials owing to characteristics of inexpensive, easy to get and low cost synthesis methods [44]. Lastly, SnO_2 nanostructures have wide band gap (3.6 eV) and large excitation energy (130 meV), therefore; these are used as n-type semiconductor material and applied for gas sensors, transparent electrodes, solar cells and supercapacitors [11-14]. Tin oxide nanostructures are extensively synthesized through several growth methods and facilitated in many application fields, however; these are rarely utilized as whiskers in carbon fiber composites.

The general properties of these three metal oxides are shown in Table 1-1. Among these metal oxides, the tin oxide has the highest value of band gap and excitation binding energy which represents that SnO_2 is the most chemically stable. ZnO exhibits highest theoretical capacitance, however, it is too insulating and presents poor rate capability and reversibility during charge/discharge process [45]. Meanwhile SnO_2 are extensively used in energy storage applications due to its realiability of pseudocapacitive behaviors while operating [63]. In addition, the bulk modulus is highest relative to ZnO and CuO. The bulk modulus is the elastic properties of material and describes the strain response to hydrostatic stress involving change in volume without shape change. The highest value of bulk modulus and advantageous characteristic in energy storage of SnO_2 are suitable for developing mulifunctional structural and energy storage composites.

Table 1-1. Properties of SnO_2, ZnO and CuO [38, 46-53]

	SnO_2	ZnO	CuO
Structure	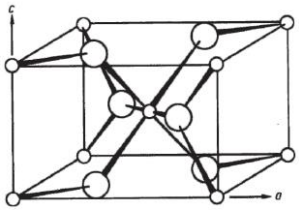	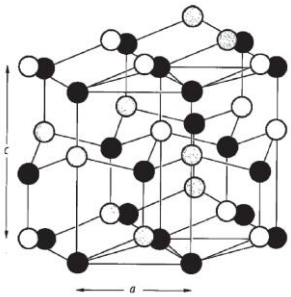	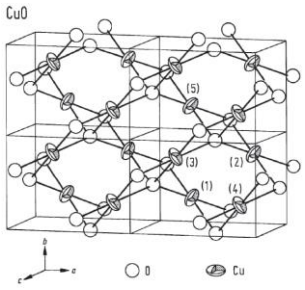
Lattice parameters	a 4.737 Å c 3.186 Å u 0.307 Å	a = b 3.249 Å c 5.2042 Å c/a 1.6018 Å	a = 4.6927 Å b = 3.4283 Å c = 5.1370 Å
Crystal structure	Rutile	Wurtzite	Monoclnic
Density (g/cm3)	6.994	5.675	6.569
Band gap (eV)	3.596	3.441	1.2
Excitation binding energy (meV)	130	63.1	-
Dielectric constant	9.58	8.75	18.1
Theoretical capacitance (mAh/g)	781	978	674
Bulk modulus (GPa)	205	183	99.7

Carbon-based materials are frequently used owing to its superior conductivity and structural performance as electrodes. The multifunctional structural capacitor built around the laminated carbon fiber layers. There are two vital components in structural capacitors. One is solid electrolyte matrix that enables ionic motion and provides sufficient structural support and interfacial bonding. The other is a functionalized electrode that contains superior energy storage capability and mechanical properties [31]. Such devices suffer performance limiting issues such as delamination at the fiber-matrix interface due to insufficient interfacial bonding. In addition, higher surface area of the electrodes results in improved energy capacitance. Therefore, the carbon fiber electrodes are used with surface modification to increase surface area and enhance the interphase interaction through deposition of nanostructured materials. Synthesizing tin oxide nanostructures on carbon fiber surface would be appropriate candidate for increasing surface area and energy storage capability (high theoretical capacitance).

In this thesis, the importance of improving the interphase condition will be emphasized for the multifunctional properties of CF (carbon fiber) composites. In addition, the tin oxide nanostructures are evaluated as secondary interphase reinforcements in CFRP composite via characterizing the structural and energy storage performances. The objective of the study is to synthesize tin oxide nanostructures on CF surface, utilize them for interphase reinforcements and characterize mechanical and energy storage performances of SnO_2-CF composite for multifunctional application.

1.5. Outline of thesis work

In the work reported here, tin oxide nanorods grown carbon fiber composite has been systematically studied. The chemical characteristics of synthesized nanorods were analyzed via SEM, XRD, XPS, and BET. The mechanical properties of SnO_2-CF composite were exhibited by impact and tensile tests. In addition, the multifunctional structural composite were fabricated with SnO_2-CF as electrodes and demonstrated electrochemical energy storage performances through CV, GV and EIS measurements.

The rest of this thesis is structured as the following.

Chapter 2 addresses the characteristics of carbon fiber reinforced composites and its application. The advantages and disadvantages of carbon fiber composites are explained and the surface treatment methods on carbon fiber surface to overcome disadvantages. In addition, the principles of the energy storage mechanisms of capacitors are explained through electric double layer models. The components will be briefly discussed are electrode, electrolyte and separator.

Chapter 3 introduces the experimental details for synthesizing tin oxide nanostructures and SnO_2 nanostructured CF composites. The characterization results are provided which involves multiple techniques such as scanning electron microscopy (SEM), X-ray diffraction (XRD) and X-ray photoelectron spectroscopy (XPS) for SnO_2 nanorods. In addition, the mechanical characterization results of composite are exhibited via impact and tensile tests, moreover, compared with other metal oxides reinforced composites.

Chapter 4 demonstrates the electrochemical energy storage performances of tin oxide functionalized structural capacitor. The SnO_2-CF electrodes surface area is analyzed by BET method for observing surface area improvement of carbon fiber electrodes. Electrochemical energy storage performances of structural capacitor are exhibited via CV, GV, and EIS tests. In addition, the energy storage performances are compared with other reported results of carbon based structural capacitors in Ragone plot.

Chapter 5 summarizes the research works and results of this thesis and several future works to improve the performance of SnO_2-CF composite are suggested.

2. Literature review

2.1. Carbon fiber reinforced composites

The importance of carbon fiber composite materials is increasing in many applications such as aerospace, automotive and other weight sensitive applications due to its superior combination of stiffness, strength, and light weight. In addition, their fatigue tolerance, chemical and corrosion resistance makes them desirable for advanced structural engineering application. The high specific stiffness and modulus can be visualized by using modified Ashby chart [54] as shown in Figure 2-1. Current applications include the Formula 1 in motorsport team of McLaren [55]. In US Air Force, the F-22 Raptor and Joint Strike Fighter consist approximately 25% composite by weight. The Committee on Materials Research for Defense After Next (2003) argued that fiber-reinforced polymer composite have the potential to achieve a 20-25% improve in performance in next 15-25 years.

Composite materials are made from two of more constituents with significantly distinctive properties to make one heterogeneous material. The composite material is composed of constituent materials that contain a reinforcement and matrix. The advantage of the composite material is that it is designed to take advantage of the beneficial properties of each constituent without being limited as much by the original constituents.

The fiber reinforcements are made through textile techniques such as braiding, weaving, and knitting. The woven fiber fabrics generally consist of two sets of yarns that are interlaced and vertically stacked to each other. The yarns that lie along the length of the fabric while the treads that lie from the other side of the fabric. The weaves are classified into three different shapes; (a) Plain weave, (b) Twill weaves, (c) Harness-Satin weaves [56] which shown in Figure 2-2.

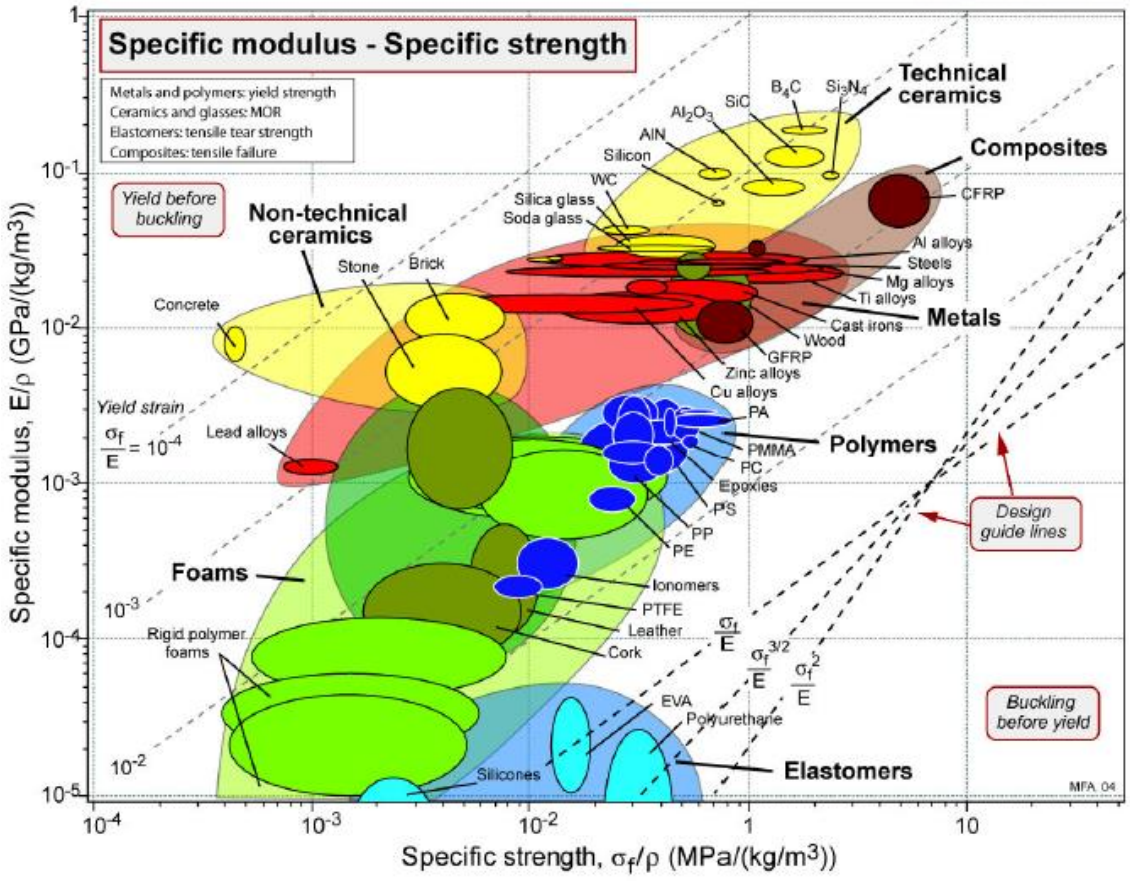

Figure 2-1. Modified Ashby materials property charts for specific modulus, against specific strength

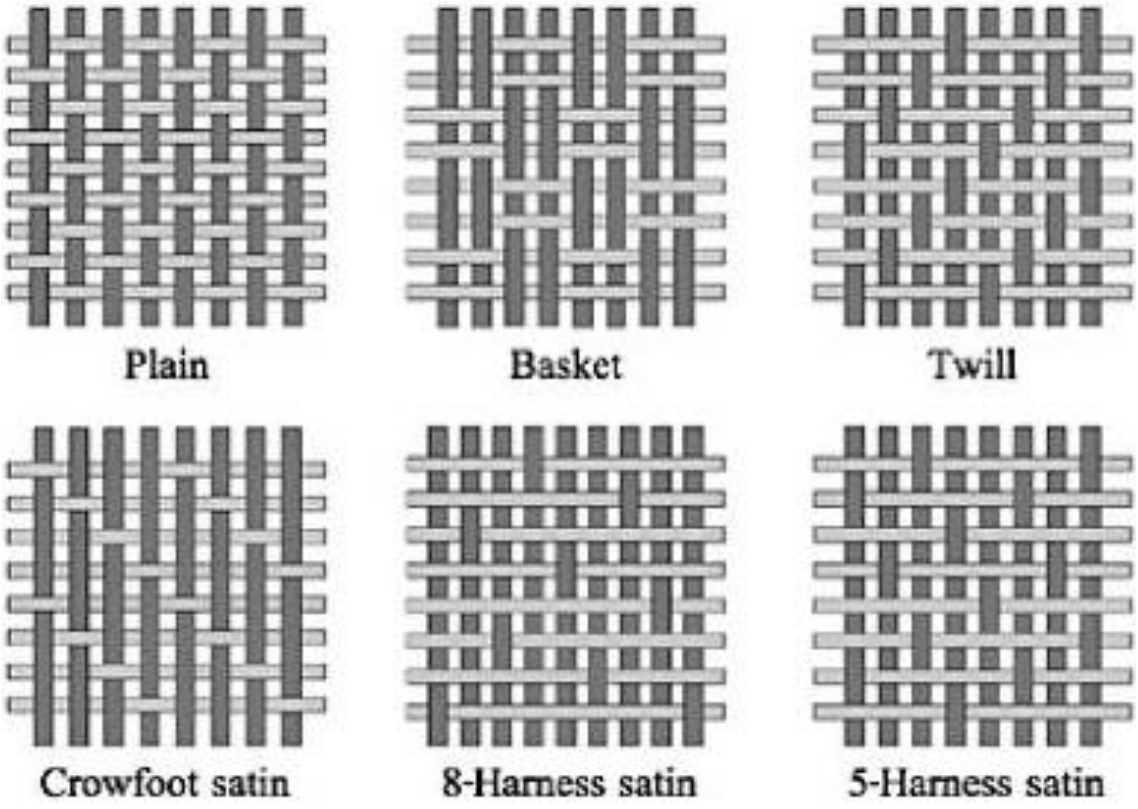

Figure 2-2. Basic weave types [4]

The plane weave (0/90) is the most common weave style and needs only four weaving yarns: two warps and two fills. The simple plain-woven fabric is highly interlaced and thus very resistive to in-plane shear movements [57]. A Harness-satin weave produces more flexible fabric than plain weave. The fill yarn floats over several warp yarns before interlacing under one. Common satin weaves are 4-Harness Satin, 5-Harness Satin and 8-Harness Satin. The twill woven laminate performs a higher tensile modulus than plain woven laminate, however, has lower tensile modulus. [58]

In manufacturing fiber reinforced composites, the polymer matrix material is introduced to the reinforcement before or after placing the fibers into the mold cavity or surface melding. There several types of manufacturing processes: pressure bag molding, vacuum bag molding, resin transfer molding, autoclave molding and vacuum assisted transfer molding (VARTM). In the case of VARTM process, the woven laminated composite is manufactured via infusion of polymer resin under vacuum state. The resin-infused fibers are placed in vacuum for several minutes or hours until resin is cured.

Despite the many attractive mechanical properties of fiber reinforced composite, they are still crucially influenced by interphase state within interlaminar region [59]. A carbon fiber composite manufactured from a strong fiber and well-suited matrix would not inevitably conclude a strong material due to the interface state between fiber-matrix is crucial in determining the mechanical properties of the final composite [60]. Besides, the whole properties of the fibers are not fully performed owing to the presence of debonding at fiber-matrix interface as shown in Figure 2-3 [61].

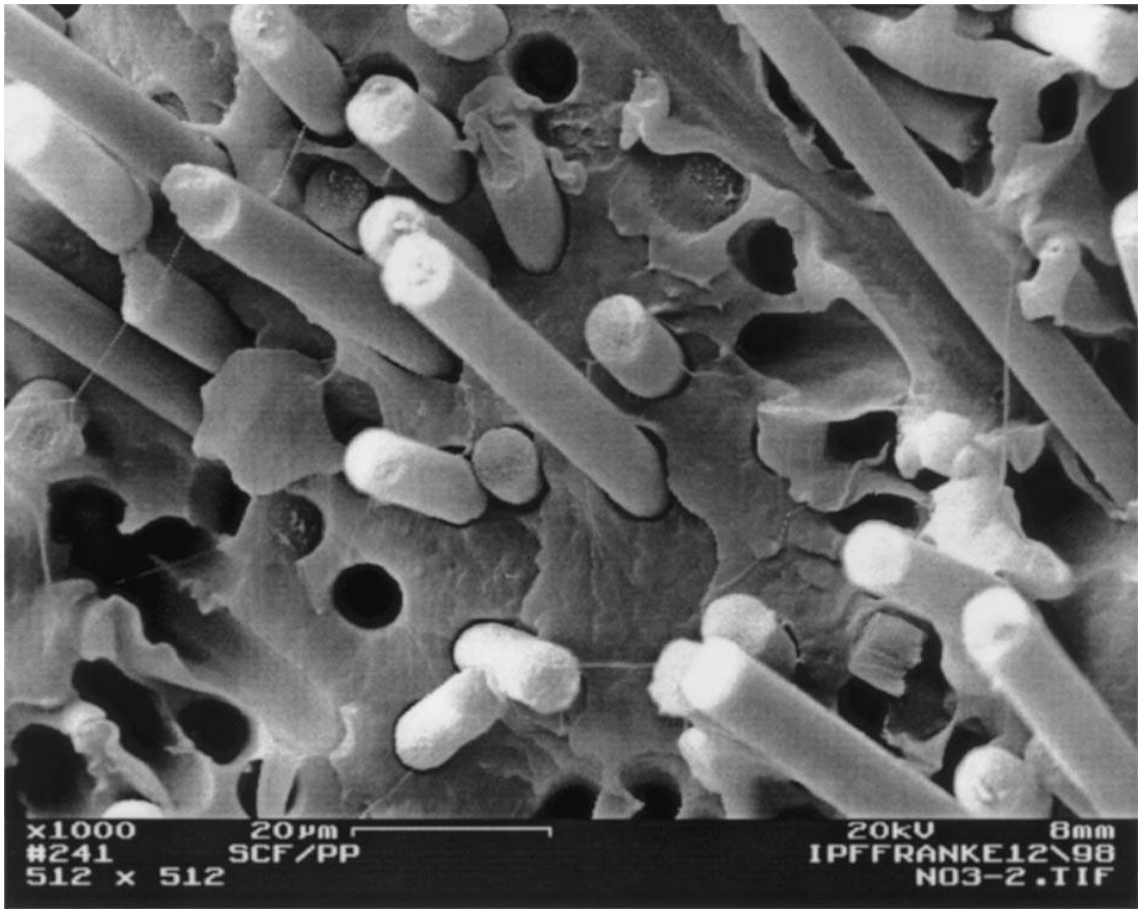

Figure 2-3. Debonding of the fibers from the matrix showing the low adhesion of fibers to matrix that reduces the strength of the composite [61]

Most carbon fibers are used with surface treated for enhancing interphase interactions with matrix via increasing the surface area and functional groups. Surface treatments can be divided into oxidative and non-oxidative treatments.

Oxidation treatments includes gas- (air, ozone, oxygen, etc.) or liquid-phase (hydrochloric acid, nitric acid etc.) oxidation through chemically or electrochemically oxidation. Gas-phase oxidation is performed at high temperatures in a gas contained environment which creates functional groups on carbon fiber surfaces. However, the surface functional groups are unstable which created by this method. The surface of the fiber may not be burned uniformly, resulting in high reactivity surface. Therefore, the reduced tensile strength and modulus are appeared by these detrimental effects. In liquid-phase oxidation (wet oxidation), the liquid oxidizing agents (chlorosulfonic acid, nitric acid etc.) are used to modify the surface. The surface functional groups such as carboxyl, ether or hydroxyl are attached onto the fibers, and thus the load transfer and adhesion within interlaminar region are improved. The concentration of agent liquid, exposure time and temperature are the factors of this process. In electrochemical wet oxidation, reactive surface and enhanced adhesion are presented by electric charge. The chemical reactions enhances the surface roughness and the wettability of the fibers, therefore, the interlaminar shear strength of the composite and mechanical interlocking in the fiber-matrix interface is improved. Although some improvements are achieved by oxidation, they also damage to the surface of the fiber and deteriorate tensile strength of the carbon fiber [62].

The non-oxidative treatments involve the deposition of more active material forms such as whiskers and nanostructures to improve the load transfer and bonding. Unlike the oxidation methods where the surface functional groups are attached, the non-oxidative treatments deposit the secondary materials as interphase. These methods are can be considered as interphase treatment due to a third constituent is inserted to the composite between carbon fibers and matrix [63]. Through introducing intermediate phase with superior structural performances such as sizings [64], SiC whiskers [65], carbon nanotubes [66], and metal oxide nanostructures [67]. In polymeric sizing interphase, the strong adhesion between the sizing layer and matrix results in failure at the interface of sizing layer/fiber. The sizing on carbon fibers are chemically compatible with the polymer and the matrix. The interfacial shear strength in the composite with sized fiber was greater than unsized fiber composite [68]. In addition, the failure mode of sized fiber composite was different because the interfacial failure is appeared from matrix cracking. On the contrary, the unsized fiber composite showed debonding between fibers and matrix [64]. The sizing of carbon fiber leads to high adhesion within interphase region and allows energy release in the interphase which improves the fatigue resistance.

A whiskerization method is growing whiskers on the fiber surface which synthesizing protrudes nanostructures into the matrix to enhance surface area, and hence, bonding and load transfer within

interphase. This process is independent to the resin system, in other words, it does not affected by chemical reaction or the affinity of the resin. The whiskers have to be tightly attached to the fiber surface in order to effectively develop improved interface strength. Two interfaces which are created by whiskerization must be stronger than previously existed one interphase. Generally, the high strength nano-crystals are grown such as SiC [65], metal oxides [67, 69] to obtain enhanced surface area and increase mechanical interlocking within interphase. Several synthesis methods for whiskerization involve chemical vapor deposition (CVD), thermal evaporation, solvothermal, and hydrothermal techniques. CVD process is the one of the common method, for instance synthesizing SiC nanostructures, and is carried out high temperature (over 1000 ℃) [65, 70]. The interlaminar shear strength was increased with CVD method; however, the in-plane properties of composite were drastically deteriorated owing to the damage of fiber by high processing temperature. Carbon nanotubes are also utilized with deposition on carbon fiber due to good mechanical properties, high aspect ratio and surface area. These can be synthesized through CVD method; however, the tensile strength can be enormously deteriorated because this method is very sensitive to small variations as shown in Figure 2-4 [71].

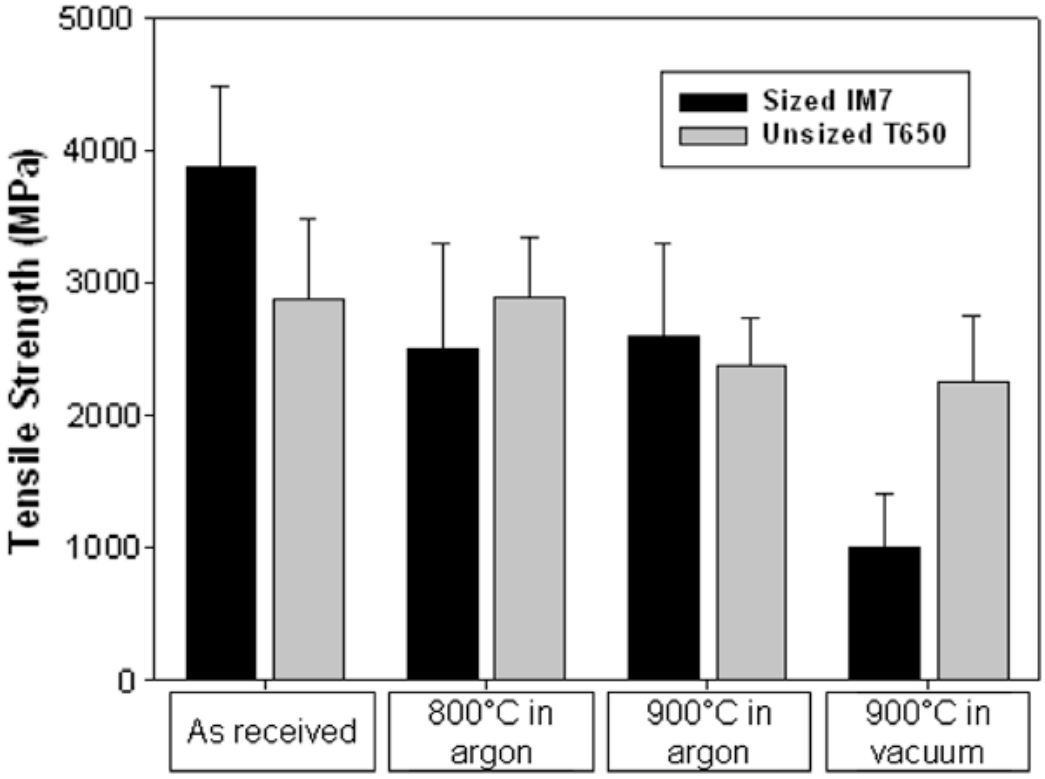

Figure 2-4. Change of carbon fiber tensile strength after synthesis of CNTs through CVD [50]

The hydrothermal technique is another whiskerization method which is promising due to low processing temperature, short reaction time, and rapid growth rate of crystal. This method is usually performed between 100-300 ℃ for several hours usually from 4 hour to few days. Although it can be considered as high temperature, actually these temperatures are relatively lower than other techniques. This low temperature nucleation does not damage to carbon fibers and thus enhanced mechanical properties of composite can be promoted. Temperature, pressure, and surfactants are used in this process in order to enhance solubility of precursor and change solution conditions for favorable formation of desired phase. In addition, this method includes several advantages such as low cost, high purity of product, and the capability of controlling the crystal size [72]. ZnO nanowires were synthesized through this method under low temperature (90 ℃) for several hours [73, 74]. The low temperature does not affect the elastic properties of the fibers and create strong interface. The synthesized ZnO nanowire presented highly increased surface area and shown 320% increase in the interfacial shear strength than carbon fiber/epoxy interface. CuO nanowires were also synthesized with this method about 100 ℃ for 12 hours [34]. The CuO nanowires on carbon fiber surface reinforced interphase interactions and hence enhanced surface area and mechanical properties of composite were performed. The strong adhesions at interphase region as well as load transfer by mechanical interlocking were appeared owing to increased surface area and surface functional groups on metal oxides.

Similarly, the tin oxide could be synthesized for whiskers on carbon fiber surface via hydrothermal method. The synthesis of tin oxide nanorods by hydrothermal method has been reported [21, 75], however, few studies have been reported as the sort of whiskers on carbon fiber surface for the composite reinforcements.

2.2. Multifunctional materials

The carbon fiber reinforced composites have been presented superior improvements and offered application opportunities to industries. More recently, the composites are considered as multifunctional materials due to its combined structures with two or more distinctive materials in one [76]. The multifunctional material can be defined that a new materials or structures perform more than two functions simultaneously. The multifunctionallity in this material can be classified into (a) multi-structural functions, (b) combined structural and non-structural functions, and (c) both. One example for type (a), the composites perform high stiffness, high strength, high fracture toughness and high impact resistance. In the case of type (b), the load-bearing structure which can provide noise and

vibration control, self-healing, thermoelectric, or energy harvesting/storage function. While an example for type (c) would be a structure which combined type (a) and (b). Recently, most of multifunctional materials are developed in type of (b).

The multifunctional materials must be composite by definition. In addition, the many achieved researches about composite have been greatly offered the capabilities for designing multifunctional materials and structures. Among them, the combination of structural and energy storage capabilities in one material, to develop structural energy storage devices, provides the capability of significant reducing the system redundancy (weight and volume) [77]. Traditional systems are relying on independent load-bearing structural and energy storage materials. Such systems are reliable to aerospace, electric automobile and portable electronics where reducing weight and volume of system could achieve superior improvements of system level performance. Optimizing structural energy materials is considerable challenge due to such functionalities are usually conflicting, often with cross-cutting phenomena [78]. However, the rewards of developing such multifunctional materials are enormous which offers significant redundancy reductions in system [32]. Previous studies have been reported multifunctional structural composites such as structural battery [79, 80], structural capacitor [27], and structural fuel cell [81]. A gel-based composite polymer electrolyte for lithium batteries was developed via utilizing hierarchical mesoporous silica network and achieved a discharge capacity as much as 150 mAh/g [79]. Nanometre-sized ceramic TiO_2 assisted polymer electrolyte for lithium battery was demonstrated conductivity around 10^{-4} S/cm at 50 ℃ and 10^{-5} S/cm at 30 ℃ in a PEO-$LiClO_4$ mixture [80]. The structural capacitors using carbon-fiber/epoxy-matrix composite was manufactured with 1.2 $\mu F/m^2$ capacitance at 2MHz [27]. The structural fuel cell was studied with solid oxide nanomaterials and mechanically tested via stretching and bending [81]. In this research, the structural capacitor is focused via facilitating carbon fiber reinforced polymer composite. Tin oxide nanostructures was synthesized on carbon fiber surface as whiskerization, in addition, this material is frequently used in energy storage applications. Therefore, the structural and electrochemical energy storage functions were evaluated by mechanical tests and electrochemical characterization.

2.3. Working principles of capacitors

2.3.1. Electrochemical capacitors

Electrochemical capacitors (EC), also known as supercapacitor comprises two high surface electrodes with a separator between them. Those two electrodes are dipped in electrolyte and separated by separator which prevents the electrical contact between electrodes and allows ion transfer. The ECs are macroscopically worked like conventional capacitors. The conventional capacitors, also known as electrostatic capacitor, are formed with two parallel electrodes which separated by a dielectric membrane as insulating layer. The capacitor performances can be characterized by capacitance C. It is the capability of charge storage which is defined by the ratio of stored charge Q to the applied potential V:

$$Q = C / V \tag{2.1}$$

The capacitance of electrostatic capacitor with vacuum layer between parallel electrodes can be estimated as follows:

$$C = \varepsilon \frac{A}{d} \tag{2.2}$$

where two electrode distance of d, vacuum permittivity of ε and electrode surface area A. The energy storage performances of capacitor are presented by energy and power of device [82]. The energy E stored in capacitor is can be obtained by utilizing eq. 2.1.

$$W = \int_0^Q V dq = \int_0^Q \frac{q}{C} dq = \frac{1}{2}\frac{Q^2}{C} = \frac{1}{2} UQ = \frac{1}{2} CU^2 \tag{2.3}$$

C is the capacitance and U is the operating potential of capacitor. The power P that capacitor is able to deliver is determined by the equation

$$P = E / t \tag{2.4}$$

2.3.2. Electric double layer

Electric double layers are generating when ECs are connected to external power supply, the positive and negative ions in electrolyte are accumulated onto the electrode surface. The balancing counter charge layers are appeared on the surface of the charged electrode. Hence, a double layer of charge is appeared at each electrode. There are several models for this double-layer interface. The Helmholtz, Gouy-Chapman, and Stern models are shown in Figure 2-5, where Ψ is the potential, Ψ_0 is the electrode potential, IHP and OHP is the inner and outer Helmholtz plane in Stern model [83].

2.3.2.1. Helmholtz model

The concept of a double-layer was first described by von Helmholtz which is the simplest theory for demonstrating the spatial charge distribution at interface. The charge of the electrode is balanced by opposite ions in a distance (d) from the surface to the center of the ions. However, the ions on the electrolyte side cannot form static compact arrangement; therefore this model could not sufficiently explain what occurs in nature [84].

2.3.2.2. Gouy-Chapman model

The Helmholtz double-layer model was modified by Gouy and Chapman. They suggested that same amount of opposite charges are appeared with charged solid surrounded in electrolyte solution and charges are not arranged compactly on to the surface [84]. The continuous distributions of ions in the electrolyte are demonstrated by a diffuse layer with distance d due to the kinetic fluctuation. The ions were assumed as point charges; therefore, they could be arranged on the surface with no limits which is untrue. This model fails for highly charged double layer which charged ions closely arranged to the electrode surface [85].

2.3.2.3. Stern model

Stern considered both the Helmholtz model and Gouy-Chapman model in order to recognize inner compact layer and diffuse layer and modified the Gouy-Chapman model by assuming ions have a finite size. In stern model, the first ions are adsorbed compactly on electrode surface, like Helmholtz model, as inner compact layer. After charges compactly adsorbed, the ions are distributed in electrolyte same as diffuse layer in Gouy-Chapman model [85]. This model has been demonstrated that the capacitance of double-layer is also influenced by the surface properties of electrode [86].

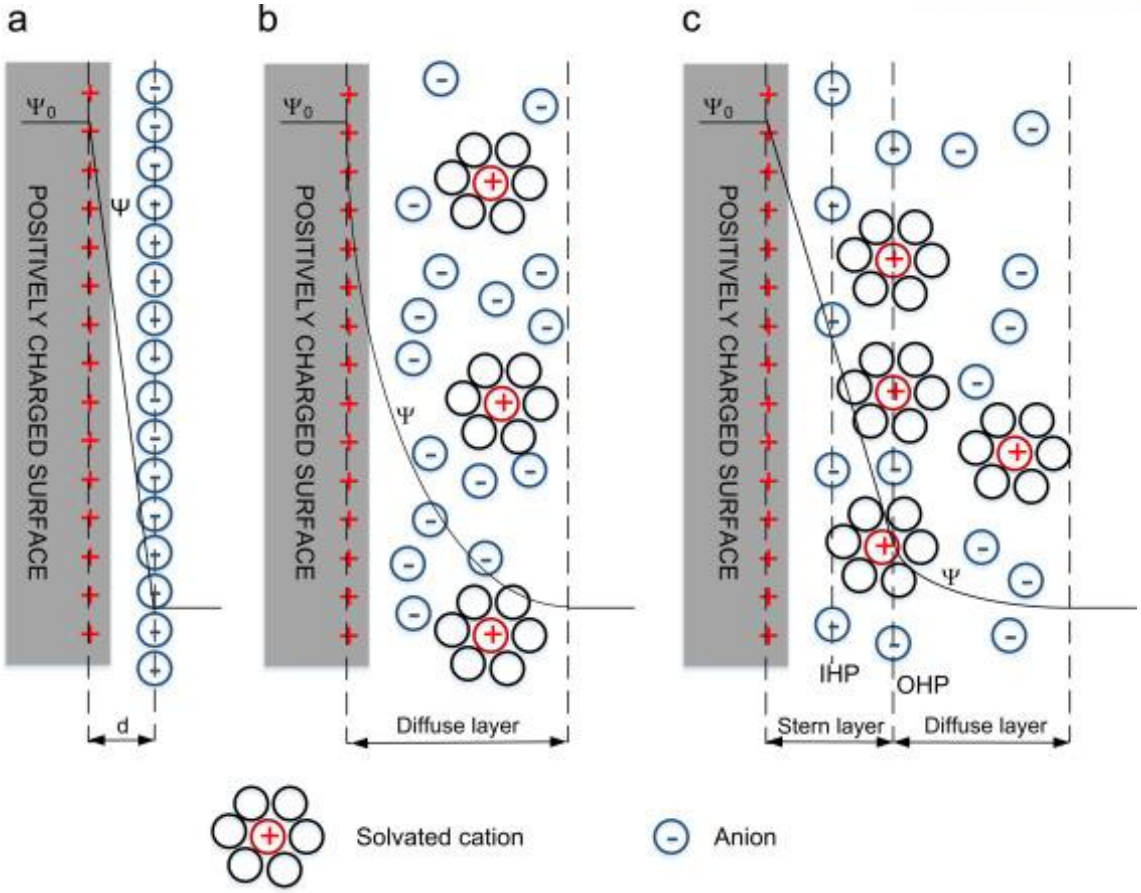

Figure 2-5. Electric double layer models, (a) Helmholtz model, (b) Gouy–Chapman model, and (c) Stern model [83]

2.3.3. Comparison of energy storage devices

The Ragone plot (Figure 2-6) presents the energy storage performances of various energy devices by energy and power density visualization [87]. Energy density determines the amount of energy could be stored in cell and power density indicates the rate of the energy could be delivered. From the plot, the conventional capacitors are considered as high power device but perform relatively lower energy density. It indicates that the rate of charge or discharge is very high but it cannot store much energy in unit mass and volume. Whereas, high energy density could be achieved in batteries or fuel cells, but depicts a poor dynamic performance. EC has the capability to store more amount of energy due to the high electrode surface area than capacitor and provides more power than batteries. Therefore, the ECs can be charged or discharged very fast and store a moderate energy. In addition, the charge storing mechanism involves only physical storage process without chemical or phase behavior; therefore, storage mechanism is highly reversible and enables large charge-discharge cycles [88]. By these reasons, ECs are appropriate candidate for the future energy storage device.

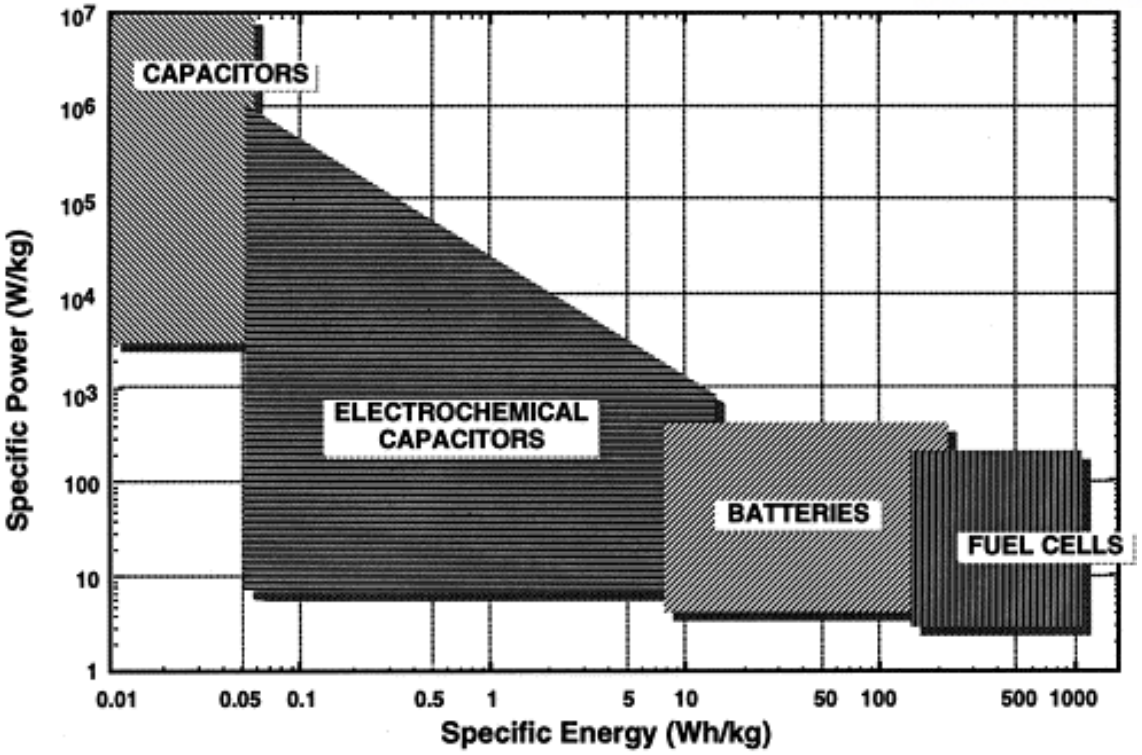

Figure 2-6. Ragone plot for various electrochemical energy storage systems [87]

2.3.4. Types of energy storage mechanism

Two different types of energy storage mechanisms can be classified into electrochemical double-layer capacitance (EDLC) and pseudocapacitance. EDLC is caused by the separation of charge at the surface of electrodes within interphase region between electrode and electrolyte, while pseudocapacitance is incurred from the fast and reversible faradic redox reactions.

2.3.4.1. Electrochemical double layer capacitance

EDLC presents similar behavior to the conventional electrostatic capacitor which non-Faradic charge storage mechanism. In non-Faradic process, there is no limitation aroused by electrochemical kinetics; therefore, it performs higher power density than pseudocapacitance mechanism, and higher energy storage capability than conventional capacitors. On applying an external voltage between electrodes, in order to maintain a neutral system, ions in the electrolyte are absorbed onto surface of the opposite charged electrode, hence the double layer structure are appeared at both electrodes. In detail, the cations in electrolyte move to the negative electrode whereas anions move towards the positive electrode. While charging process in the positive electrode:

$$E_{+} + A^{-} \rightarrow E_{+}^{+} // A^{-} + e^{-} \tag{2.5}$$

E_+ is the positive electrode, A^- is the anion and // is the interface between electrode and electrolyte. At negative electrode:

$$E_{-} + C^{+} + e^{-} \rightarrow E_{-}^{-} // C^{+} \tag{2.6}$$

E- is the negative electrode, C+ is the cation. The discharge process is reverse of above the equation. High surface area materials are utilized for electrode due to shorter distance between electrode and electrolyte.

The equivalent circuit of an EDLC cell is shown in Figure 2-7. R_p is the resistance of the insulating layer and assumed to be large enough. In double layer region, the capacitance and resistance are maintained at same voltage, thus the circuit presents a parallel relation of C_{dl} and R_p. Besides, the resistance also exists in adjoining regions such as electrolyte, electrode and current collector; therefore, this resistance is presented as R_s [89].

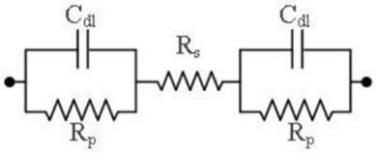

Figure 2-7. Equivalent electrical circuit of an EDLC cell [89]

2.3.4.2. Pseudocapacitance

A pseudocapacitance presents a intermediate behavior between a battery and an electric double layer capacitor. Charge storage occurs by chemical and electrochemical means. It is not only a charge accumulation on electrode surface but also involves reduction-oxidation (redox) reactions. When external electric load is engaged, a fast and reversible redox reaction occurs on the electrode surface. Whereas the charge transfer are aroused in bulk of electrode in battery, the charge storage is takes place at the surface of electrode, thus the transfer rate is higher. During the charge process, the reaction at the positive electrode could be estimated as follows:

$$E_{+} + A^{-} \rightarrow E_{+}^{\delta+} // A^{-} + \delta e^{-} \tag{2.7}$$

At negative electrode:

$$E_{-} + C^{+} + \delta e^{-} \rightarrow E_{-}^{\delta-} // C^{+} \tag{2.8}$$

E+ and E- are positive and negative electrodes, A- is anion and C+ is cation. // presents the electrode-electrolyte interface. The δ is the electrosorption valence which related to the redox reaction in electrode.

The pseudocapacitance can be aroused by thee electrochemical features such as underpotential deposition, redox pseudocapacitance, and intercalation pseudocapacitance [90]. The first two processes are critically depends on the electrode surface area and third is mainly a bulk process. The faradic reaction incurred by the redox or doping/dedoping process of electrode and the charge transfer process is voltage dependent in pseudocapacitive behavior [91]. The redox reaction is slower than EDLC process due to the impedance of the reaction [92]. However, the much large capacitance can be achieved due to the Faradic reaction [93].

The equivalent electrical circuit of pseudocapacitance behavior is presented in Figure 2-8. C_{φ} is the pseudocapacitance, RF is the resistance between electrode and electrolyte, and RD is the Faradic resistance which may act during discharge when the ions desorb. The pseudocapacitance is larger than double layer capacitance at certain potentials and the parallel combination of this pseudocapacitance assists the capacitance development [94].

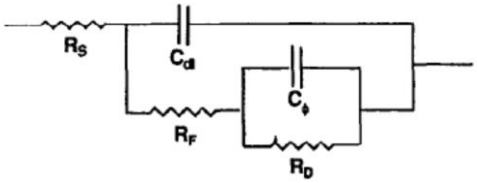

Figure 2-8. Equivalent electrical circuit of a Pseudocapacitor [94]

3. Synthesis and characterization of tin oxide nanorods on carbon fibers

3.1. Materials and reagents

T-300 grade of WCFs (woven carbon fibers) were received from Amoco Corp. (Chicago, IL, USA). Tin oxide nanostructures were grown from obtained WCFs. These nanostructures were synthesized from Tin acetate ($Sn[IV](CH_3CO_2)_4$), sodium stannate trihydrate ($Na_2SnO_3 \cdot 3H_2O$) and sodium hydroxide (NaOH) which purchased from Sigma-Aldrich (St. Louis, MO, USA). The two kinds of ethanol were utilized, one was purchased from J.T. Baker (Phillipsburg, NJ, USA) for seeding solution and the other was receieved from Samcheon Pure Chemical Co. Ltd. (Pyeongtaek, Korea) for hydrothermal process. The vinyl ester resin (RF-1001MV) and methyl ethyl ketone peroxide (MEKP) crosslinker were purchased from CCP composites (Jeollabuk-do, Korea) and ARKEMA (Gyeongsangbuk-do, Korea), respectively.

3.2. Experiments

3.2.1. Preparation of SnO_2 seeding solution and growing solution

Carbon fiber surfaces were functionalized by tin oxide nanorods as whiskers. Tin oxide nanostructures are synthesized using two-step hydrothermal method that consisting seeding and growing procedure. The tin [Ⅳ] acetate and sodium hydroxide were used for seeding procedure. Tin acetate (0.04M) was dissolved in 400mL of ethanol (received from J.T. Baker) for 30 min stirring at 65℃ heating. Sodium hydroxide (0.04M) was also dissolved in 80 mL of ethanol and dissolved solution was added to the synthesized $Sn[IV](CH_3CO_2)_4$ solution. 320 mL of ethanol was added to mixed solution for adjusting 800 mL of final seeding solution with 40 min stirring. The pH level of seeding solution was kept at 7-8. The chemical reactions in SnO_2 seeding solution were as follows:

$$Sn^{4+} + 8OH^- \leftrightarrow \left[Sn(OH)_8\right]^{4-} \tag{3.1}$$

$$\left[Sn(OH)_8\right]^{4-} \leftrightarrow SnO_4^{4-} + 4H_2O \tag{3.2}$$

$$SnO_4^{4-} + 2H_2O \leftrightarrow SnO_2 + 4OH^- \tag{3.3}$$

$$SnO_2 + 2OH^- \leftrightarrow Sn(OOH)_2^{2-} \tag{3.4}$$

The sodium stannate trihydrate, sodium hydroxide and ethanol (Samcheon Pure Chemical) were

used for growing procedure. The $Na_2SnO_3 \cdot 3H_2O$ and NaOH were mixed at a 1:4M ratio in deionized water (DIW). For preparing 10mM of SnO_2 growing solution, $Na_2SnO_3 \cdot 3H_2O$ (10mM) and NaOH (40mM) were each dissolved in 150 mL of DIW for 10 min stirring. These two precursor solutions were mixed together for 20 min stirring to obtain 300 mL of transparent solution. Then, the 300 mL of ethanol was slowly added to prepared solution with vigorous stirring for 1 hour. The pH level of growing solution was maintained at 13-14. Same procedures were followed to prepare 30, 50 and 70 mM growing solutions. As concentration of growing solution increasing, the white precipitates are appeared and white suspensions are formed. These final growing solutions were used for synthesizing SnO_2 nanorods on the treated carbon fibers. The chemical reactions occurred in the growing solution and synthesis of SnO_2 nanorods were as follows:

$$Na_2SnO_3 + H_2O \leftrightarrow SnO_2 + 2NaOH \tag{3.5}$$

$$Sn(OH)_4 + 2OH^- \leftrightarrow \left[Sn(OH)_6\right]^{2-} \tag{3.6}$$

$$\left[Sn(OH)_6\right]^{2-} \xrightarrow{\Delta} SnO_2 + 2H_2O + 2OH^- \tag{3.7}$$

3.2.2. Fabrication of SnO_2-WCF composites

80 mm x 80 mm square size of CFs was immersed in ethanol for 1 min and dried in oven at 100 ℃ for 10 min to remove the impurities from the surface of carbon fiber. These clean CFs are dipped into the prepared seed solution for 10 minutes and then annealed in furnace (Thermo Fisher Scientific Inc., Massachusetts, USA) to enhance adhesion between carbon fiber surface and tin oxide nanostructures. The soaking and annealing process were repeated for several cycles to coat $Sn(OOH)_2^{2-}$ sources uniformly on CF surface. Subsequently, the seeded CFs were dipped in prepared growing solution and kept in a stainless-steel teflon autoclave heated at 220 ℃ for 24 hours in oven. After the hydrothermal process, the SnO_2-CF sample was cleaned with distilled water to stop further growth of SnO_2 nanorods and dried at atmospheric temperature for 1 day. Samples of different growth molar concentrations were prepared to observe the effects of SnO_2 NRs on surface morphology and mechanical properties. The VARTM process was involved to prepare the final composite manufactured from SnO_2-CFs laminates and polymer resin. The overall process of synthesizing SnO_2 nanorods and fabricating SnO_2-CF composites are shown at Figure 3-1 [95].

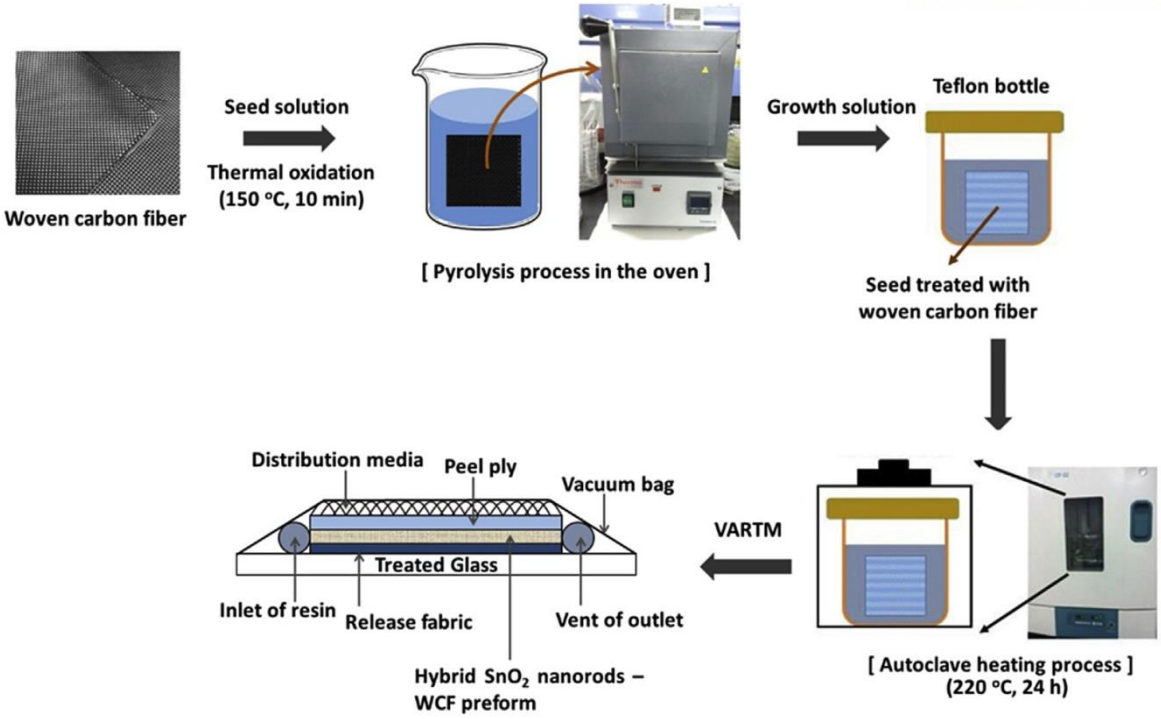

Figure 3-1. Schematics of SnO_2 nanorods grown woven carbon fiber composites [95]

3.3. Experimental results and discussions

3.3.1. Morphology analysis

Scanning electron microscopy (SEM; S-4800, Hitachi High-Technologies Corp., Tokyo, Japan) was used for observing the surface morphology of the tin oxide nanostructured carbon fibers samples. The experimental conditions (three-level, four-factor Taguchi method) were formulated to finding optimal tin oxide nanorods growing condition levels. The designed conditions and their results are listed in Table 3-1 [95] and SEM images are shown at Figure 3-2 [95]. The growth of tin oxide nanorods was critically influenced by hydrothermal growing temperature and time; however, seed cycle was not crucial parameters for the SnO_2 nanostructure growth. There was no growth of tin oxide nanorods at sample 1 due to the insufficient heating temperature and time. Samples 4 and 7 shows no growth because of insufficient heating temperature of 140 ℃ and also samples 6 and 8 failed due to the short heating time of 12 h. Result in sample 6 shows some crystallizations, however, it was deficient for enabling growth of SnO_2 NRs.

Thus, the optimal growing condition for tin oxide nanorods could be determined. The seeding cycle was not crucial parameter; therefore, it was fixed at 5 seeding cycle (middle level). The optimum level of growing temperature and time was determined at 220 ℃, 24h which is same condition with sample 3. To achieve successful growth of 1-D axial tin oxide nanorods, 5 seeding cycle, 220 ℃ of hydrothermal temperature and 24 h of hydrothermal time are necessary.

Figure 3-3 [95] shows the result of SEM images at different molar concentration with fix hydrothermal temperature and time at optimal level. The rutile structured tetragonal shaped tin oxide nanorods were grown on carbon fiber surfaces under different concentrations from 10mM to 70mM. At the optimum level of temperature and time, the size of tin oxide nanorods are measured as follows: 240.98 ± 77.59 nm in length and 188.02 ± 29.42 nm in diameter, 305.17 ± 49.22 nm in length and 167.23 ± 17.75 nm in diameter, 607.21 ± 44.67 nm in length and 98.03 ± 9.98 nm in diameter, 711.31 ± 11.71 nm in length and 80.73 ± 16.34 nm in diameter. In addition, the measured aspect ratio was 1.28, 1.82, 6.19 and 8.81 from 10 mM to 70 mM.

Judging from the growth result, two key factors of successful tin oxide nanorods growth could be identified. The first key required factor was the presence of solid nuclei in supersaturated growing solution. . SnO_2 nanostructure was grown only at the supersaturated solution by tin (Sn) solid precursor. The nucleation of SnO_2 nanostructure was initiated from amorphous Sn precipitate, proper temperature and time. In addition, the crystallization process was influenced by the number of $Sn(OH)_4$ and $(Sn(OH)_6)^{2-}$ nuclei in growing solution and hydrolysis ratio. The sufficient degree of

supersaturated Sn precursors resulted in the greater SnO_2 NRs growth due to the lower activation energy for crystallization. [96] Second, the molar ratio of Sn^{4+} and OH^- was the critical factor, in other words, pH determines the tin oxide crystalline morphology. Under hydrothermal condition, the solid nuclei underwent Ostwald ripening that is general growing process for most metal oxides. Typically, Ostwald ripening makes spherical nanostructure which is most stable in thermodynamic sense. At high pH over 13, however, the nanostructures prefer to grow in [001] direction. The surface energy is different with surface direction and increases in the order of (110) < (100) < (101) < (001), in other words, SnO_2 nanostructures preferred to form in c-axis direction. The different theoretical surface energy has been calculated by several researchers [97, 98]. Pal et al. [99] suggested that spherical morphologies are shown at pH < 11 and the crystal growth in specific orientation occurred at pH > 11. Especially, they reported the morphology transformation from isotropic spherical to 1D anisotropic shape at pH 13. As adjusting the number of Sn precursors and heating temperature and increasing hydrothermal time, the size of tin oxide NRs and surface-to-volume ratio were changed [100].

Table 3-1. Experimental conditions and results for tin oxide nanorods [95]

	Seed Cycle	Growth temperature (℃)	Growth Time (h)	Growth concentration (mM)	Result
1	3	140	12	30	Fail
2	3	180	18	50	Success
3	3	220	24	70	Success
4	5	140	18	70	Fail
5	5	180	24	30	Success
6	5	220	12	50	Fail
7	7	140	24	50	Fail
8	7	180	12	70	Fail
9	7	220	18	30	Success

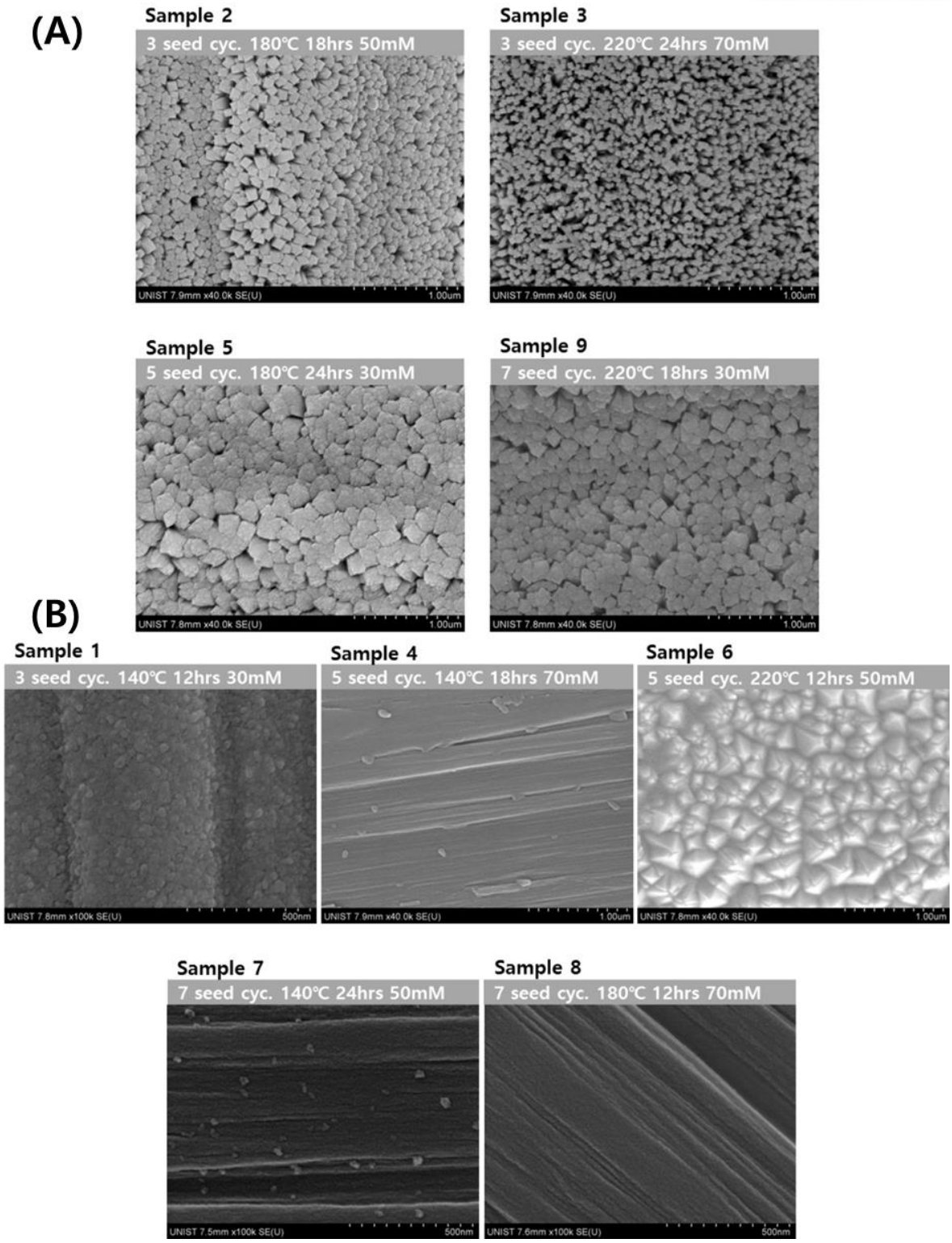

Figure 3-2. SEM images of SnO_2 nanostructures grown on woven carbon fiber after different experimental conditions. The (B) images show acceptable SnO_2 growth and the (A) images depict insufficient SnO_2 growth. [95]

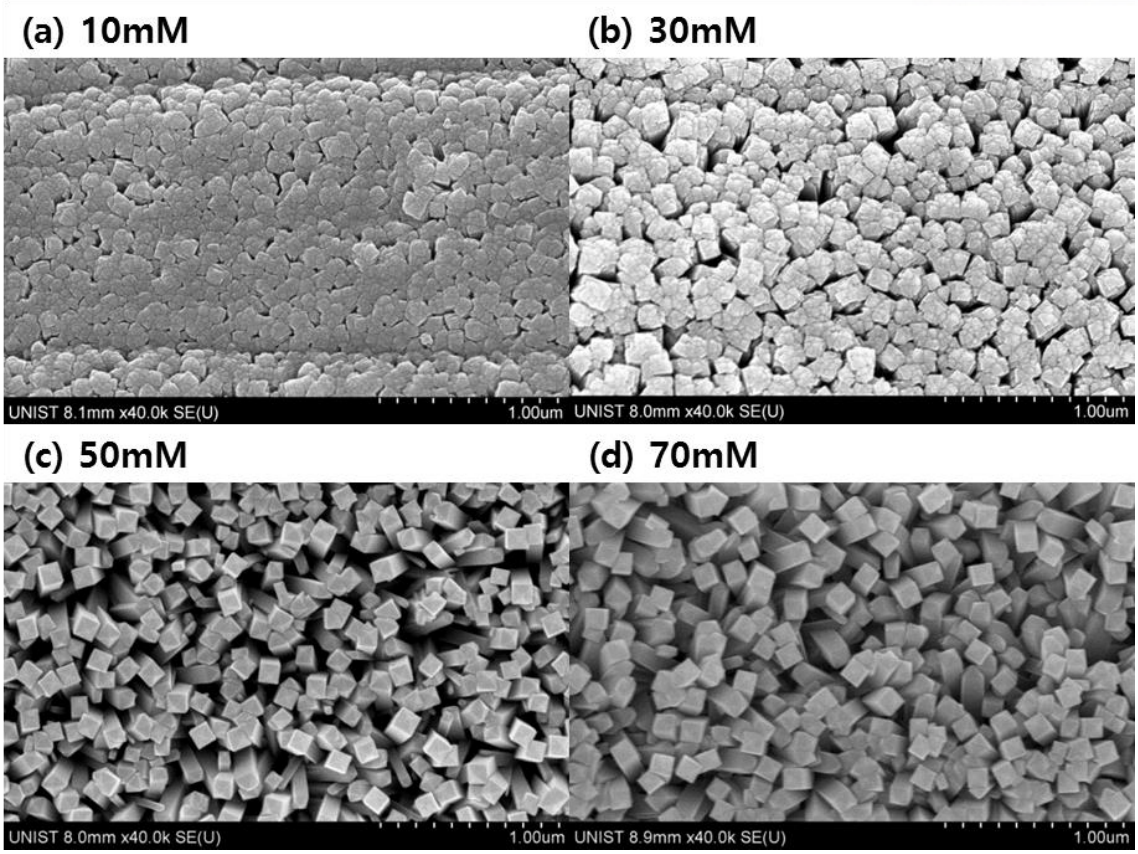

Figure 3-3. SnO_2 nanorod (NR) growth on carbon fiber surface. (a) 10mM, (b) 30mM, (c) 50mM and (d) 70mM of SnO_2 NRs. [95]

3.3.2. XRD and XPS studies

XRD was carried out using D8 advance (Bruker, Madison, USA) using crystal-monochromated Cu-Kα radiation (λ= 2.5406 Å) for 2θ = 20~80˚ with 40 kV accelerating voltage and 200 mA current. Figure 3-4 [95] show the XRD results of the as-grown nanorods and pristine carbon fiber (SnO_2 = 0 mM). All the diffraction peaks of as-prepared SnO_2 NRs can be indexed to the tetragonal structure of SnO_2 material. The lattice parameters of rutile structured tin oxide are a = b = 4.738 Å and c = 3.185 Å which well matched with the standard crystalline data from JCPDS card (41-1445). The absence of byproduct peaks demonstrates that high purity of the SnO_2 nanorods. The enhanced (002) diffraction peak represents that the oriented growth direction of tetragonal SnO_2 nanorods in [001] direction [101]. The broader diffraction peaks at 10-30mM samples demonstrate that relatively small and thick SnO_2 particles. 50-70 mM samples represent sharper and more intense peak which indicate increased SnO_2 crystallinity and higher orientation degree of NRs.

For identifying the chemical bonds configuration and composition of as-grown SnO_2 NRs arrays, the XPS (Thermo Fisher Scientific, UK) was performed and its results are shown in Figure 3-5 [95]. The Sn 3d binding energy spectra data (Figure 3-5 (A)) represent that Sn $3d_{5/2}$ and Sn $3d_{3/2}$ which peaks occurred at 487.07 and 495.47 eV, respectively. The energy difference between these two peaks was 8.4 eV, which is well matched with reported for SnO_2 nanorods [102]. The C 1s spectrum data which consisted with C-O and C=O peaks is presented in Figure 3-5 (B). These results indicate that carbon fiber surfaces are bonded with nanostructures with a good adhesion. [103] The XPS O 1s line is shown in Figure 3-5 (C) and depicts that the O-Sn4+ bonding at 530.9 eV. Therefore, O 1s line peaks demonstrates that the synthesized nanostructures are composed with SnO_2 while the O_{chem} could be indexed with NaOH (532.8 eV) or H_2O (532.8 eV).

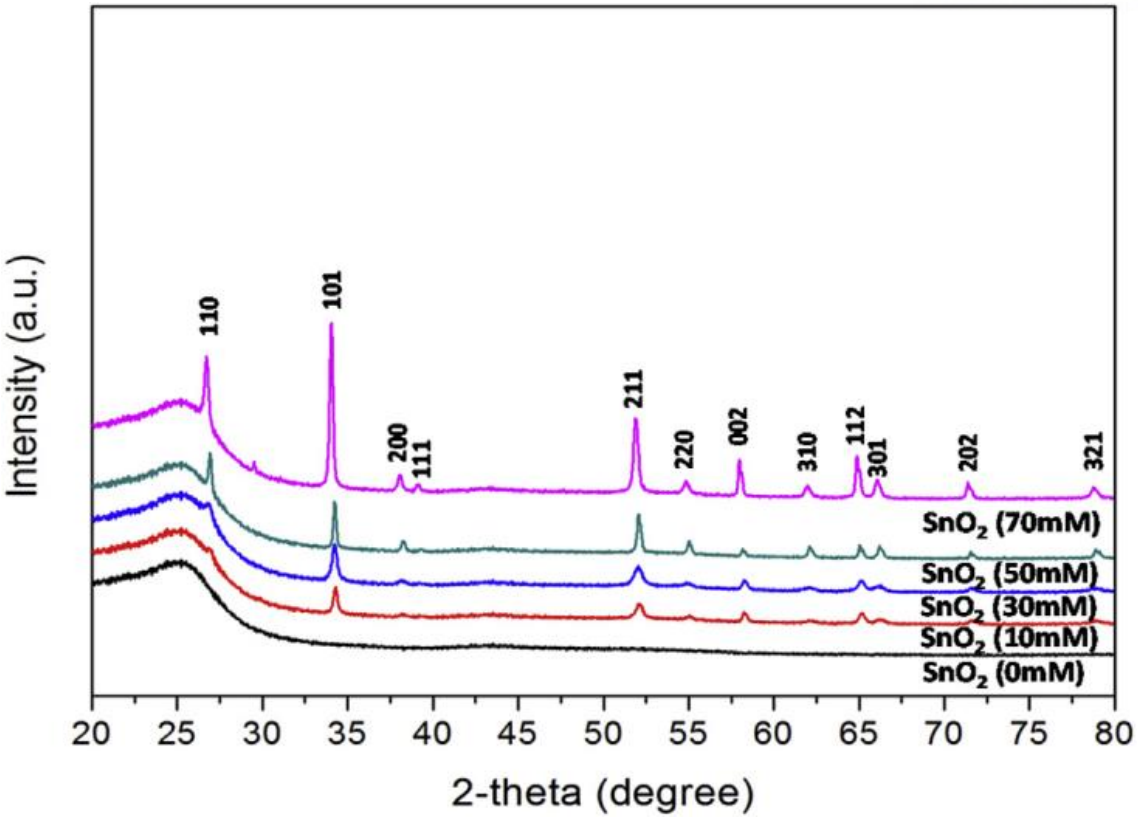

Figure 3-4. X-ray diffraction peaks for SnO_2 NRs on carbon fiber surface [95]

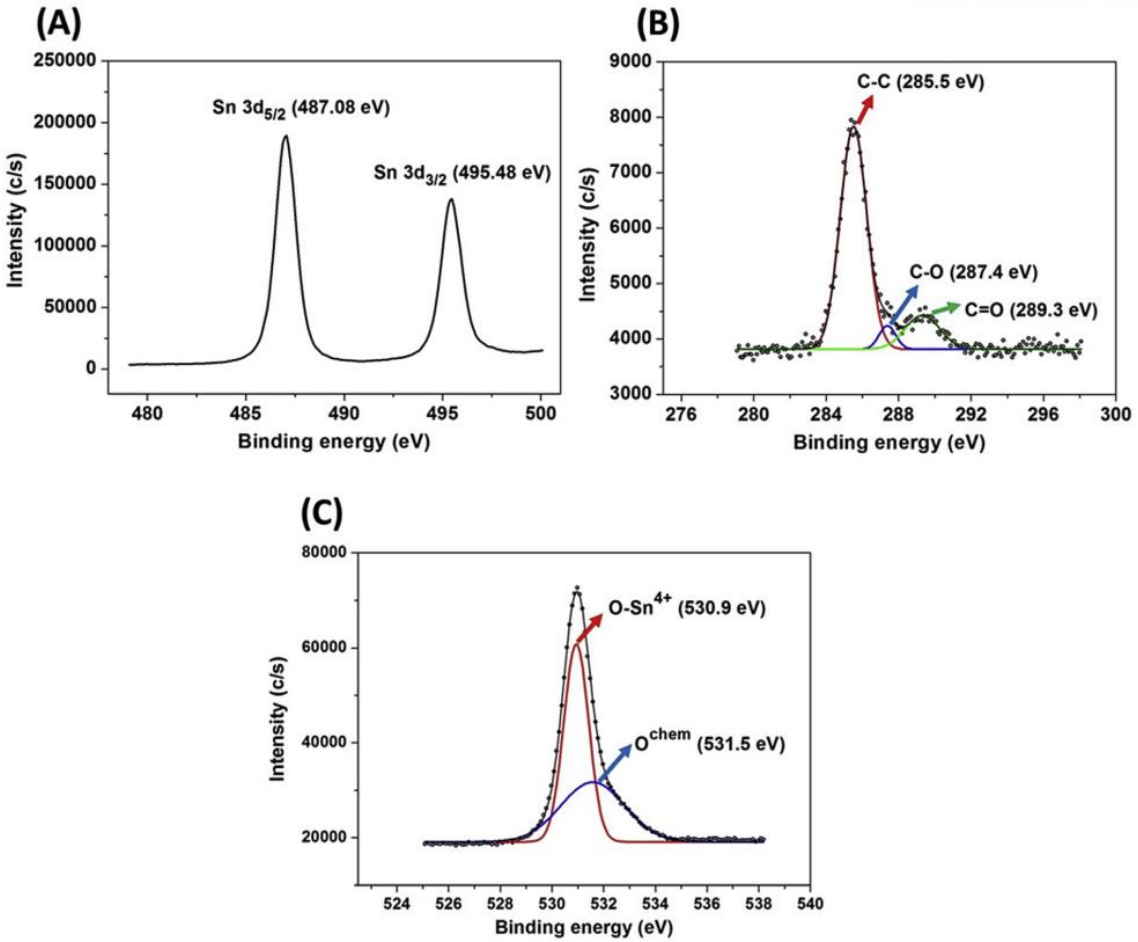

Figure 3-5. XPS results of SnO_2 NRs embedded on carbon fiber surface. (A) The Sn 3d peak. (B) The C-O, C-C and C=O peaks. (C) The O-Sn^{4+} peaks. [95]

3.3.3. Tensile tests

Tensile test was performed to evaluate the stiffness of the SnO_2-CF composite using an Instron 5982 universal tester. SnO_2 NRs were considered as secondary reinforcements at interphase region which is between matrix and carbon fiber surface.

The uniaxial tensile test was carried out for characterizing ultimate tensile strength and elastic modulus according to ASTM D3039 standard. Figure 3-6 (a) shows the tensile strength and elastic modulus in terms of SnO_2 NRs contents. The bare carbon fiber composite (SnO_2 = 0 mM) shows the lowest strength and modulus values, namely, it has the lowest interactions between matrix and fiber surface. In Figure 3-6 (a), the % increments of the ultimate tensile strength and elastic modulus were calculated which compared with the bare carbon fiber composite. As the SnO_2 nanorods were embodied into the interphase region, the ultimate tensile strength and elastic modulus are increased. In other words, the as-grown tin oxide nanorods enhanced the interphase interactions between matrix and fiber surface as secondary reinforcements. In the in-plane shear response was investigated and followed by the ASTM D3518/D3518M-13 standard method (shown in Figure 3-6 (B)). The in-plane shear strength results are shown at Figure 3-6 (B) and were determined by following equation.

$$\tau_{12}^{m} = \frac{F^{m}}{2 \cdot b \cdot d} \tag{3.8}$$

where τ^{m}_{12} is in-plane shear stress, F^{m} is maximum load, b is specimen width, and d is specimen thickness. SnO_2 nanorods on this work improved the in-plane shear strength of the hybrid SnO_2-CF composite. The SnO_2 nanorods network facilitated the load transfer via strong interactions of ionic and polar behavior of tin oxide nanorods with surface functional groups (hydroxyl, carboxyl and carbonyl). The results obviously demonstrates that the presence of the interlocked SnO_2 NRs interactions enhanced the mechanical properties (ultimate tensile strength, elastic modulus, in-plane shear strength) and could prevent the fibers from breaking.

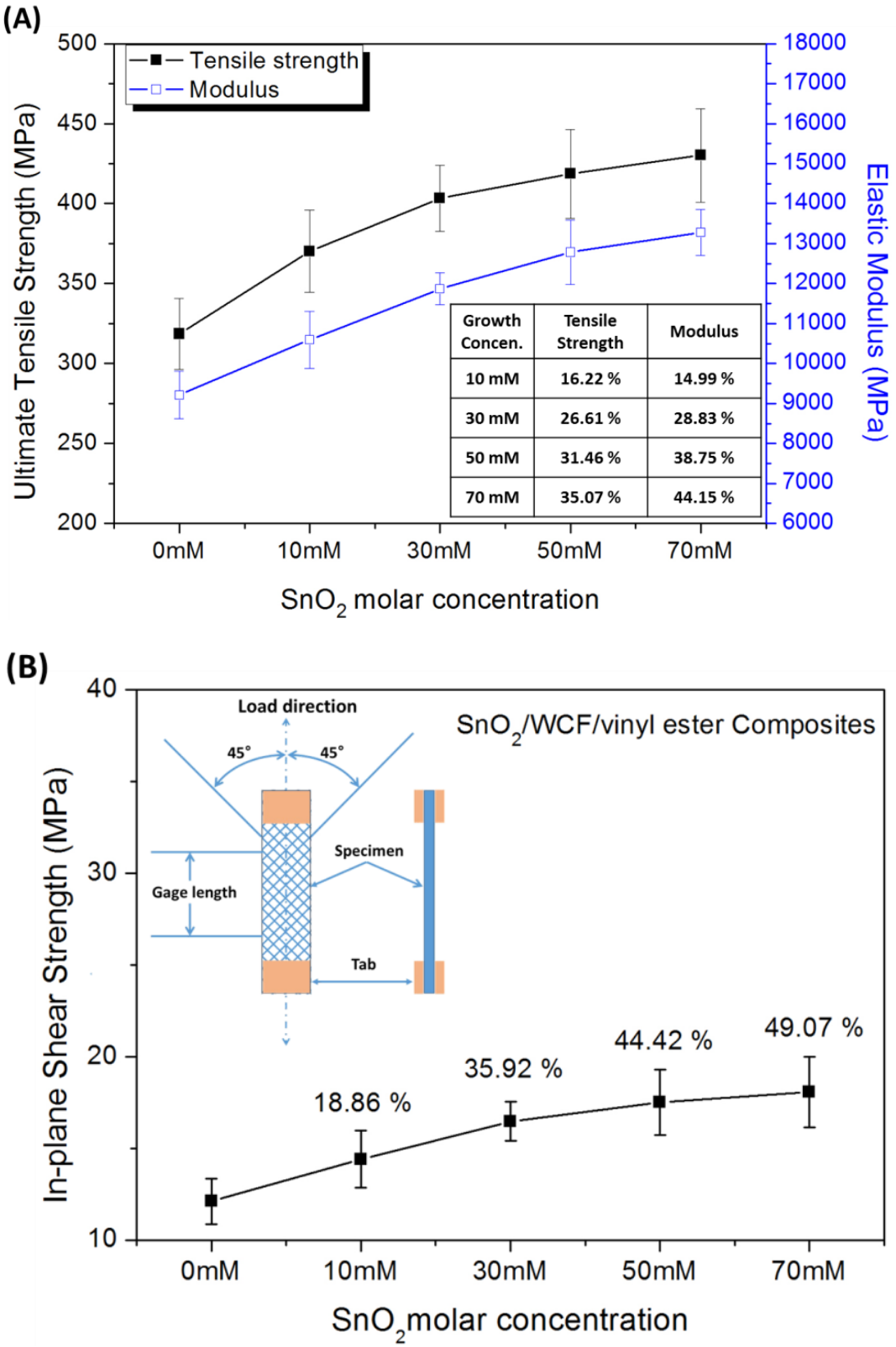

Figure 3-6. Mechanical properties of the tin oxide nanorods-WCF composites in terms of SnO_2 molar concentration [95]

3.3.4. Impact tests

For characterizing the impact energy absorption of the SnO_2-CF polymer composite, instrumented drop-down impact tester was employed. Samples were 40 mm in diameter for observing the impact absorption ratio. A photoelectric sensor collected the data from the initial impact moment until penetration occurred.

The increased specific toughness was reported via growing metal nanowires [104] and carbon nanowires [105] on polyurethane substrate. Therefore, impact absorption energy study was carried out through drop-down impact tester. The impact absorption energy has been estimated from the weight capacity of the tester at the maximum impact. Both rebound and absorbed energy are considered for determining the impact energy. When the whole energy was completely absorbed to matrix and fibers, the rebound energy could be disregarded. In case of low velocity impact, the absorbed impact energy includes the delamination and bending deformation energy. When the fiber breakage occurs, however; the inherently brittle characteristic of composite results in the medium levels of energy absorption. The measured impact energy absorption results for bare carbon fiber and SnO_2-CF resin composite are shown in Figure 3-7 [95]. The bare carbon fiber composite indicated the lowest impact energy absorption. The increased energy absorption was shown as increasing the content of SnO_2 NRs on the carbon fiber surface due to the enhanced interphase interactions within composite. These interactions led to enhanced interwinded entanglement between carbon fibers and matrix, which facilitates the absorbing and transferring the energies through the interfaces. The nanostructured tin oxide prevents the crack propagation while external impact applying via strong interlocked and adhesive networks within interfacial region. The strong ionic bonds of tin oxide nanostructures with surface functional groups of carbon materials have been reported. Xie et al. [106] and Jiang et al. [107] mentioned that strong couplings between SnO_2 and GO which developed by tightly joined Sn^{4+} onto the GO surface due to the electrostatic interactions of GO functional groups (carboxyl, hydroxyl and epoxy groups). Similarly, carbon fiber functional groups are carboxyl, hydroxyl and carbonyl, and hence the Sn^{4+} ions in SnO_2 surface interact with the hydroxyl and carboxyl functional groups at carbon fiber surface. These surface functional groups acted an important role in enhancing the properties via forming strong ionic bonds with SnO_2. Moreover, ester groups of polymer resin could interact with CF functional groups through building strong bonds. Thus, the combined effects of these various parameters enhanced overall impact energy absorption of the composite.

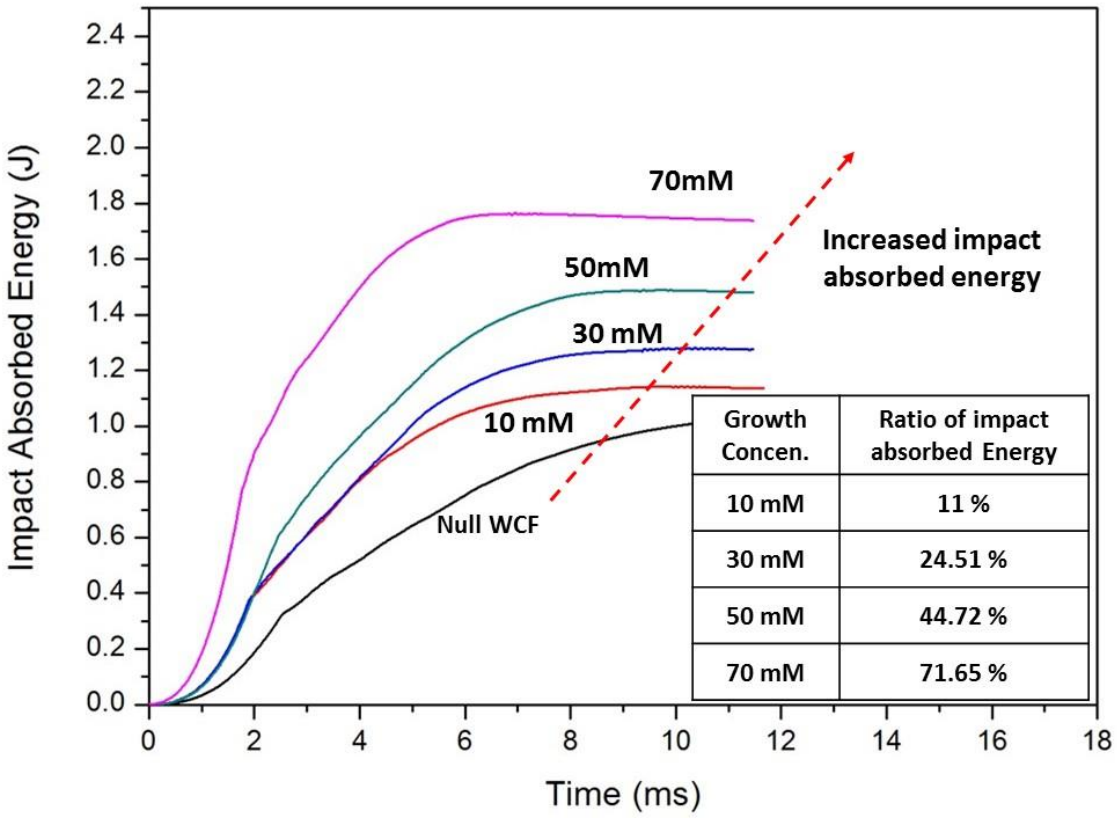

Figure 3-7. Energy-time response curve in terms of SnO_2 molar concentrations. [95]

4. Electrochemical characterization of tin oxide nanorods based solid-state capacitor

4.1. Materials and reagents

T-300 grade of plain woven carbon fibers (Chicago, IL, USA) were used for the electrode materials. A woven glass fiber (JMC Corp. Korea) was utilized as separator material which sandwiched between two WCF electrodes. SnO_2 nanorods were grown for enhancing the surface area of electrodes. These tin oxide nanostructures were prepared from Tin acetate ($Sn[IV](CH_3CO_2)_4$), sodium stannate trihydrate ($Na_2SnO_3 \cdot 3H_2O$) and sodium hydroxide (NaOH) which received from Sigma-Aldrich (St. Louis, MO, USA). The two kinds of ethanol were used as solvent, one was purchased from J.T. Baker (Phillipsburg, NJ, USA) for seeding solution and the other was purchased from Samcheon Pure Chemical Co. Ltd. (Pyeongtaek, Korea) for hydrothermal process. The unsaturated vinyl ester resin (RF-1001MV) and methyl ethyl ketone peroxide (MEKP) crosslinker were purchased for developing matrix from CCP composites (Jeollabuk-do, Korea) and ARKEMA (Gyeongsangbuk-do, Korea), respectively. The ionic liquid 1-ethyl-3-methylimidazolium tetrafluoroborate (EMIMBF4; reagent grade; C-TRI, Korea) and lithium salt lithium trifluoromethane sulfonate (LiTf) (Sigma–Aldrich, St. Louis, MO, USA) were utilized for enhancing of ionic conductivity to matrix.

4.2. Experiments

4.2.1. Solid-state capacitor assembly

The CF electrode surfaces were increased surface area via synthesizing tin oxide nanorods. two-step hydrothermal process was performed to grow tin oxide nanostructures. two-step hydrothermal process is composed with seeding and growing procedure. Tin acetate (0.04M) and sodium hydroxide (0.04M) were used for making seed solution. Both were stirred for 30 min at 65℃ heating in 400 mL and 80 mL of ethanol, respectively. Prepared two solutions were mixed after cooling and additional 320 mL of ethanol was added with stirring 10 min. The pH level of seeding solution was maintained to 7-8. The sodium stannate trihydrate, sodium hydroxide and ethanol (Samcheon Pure Chemical) were used for growing procedure. The $Na_2SnO_3 \cdot 3H_2O$ and NaOH were dissolved at a 1:4 M ratio in 150mL deionized water (DIW), respectively. Both two solutions were mixed for 15 min and then 300 mL of ethanol was slowly added for 1 h stirring. The pH level of growing solution was maintained to 13-14.

The pristine CFs were dipped in synthesized seeding solution for 10 min and then annealed at 150 ℃ for 10 min. The dipping and annealing procedures were repeated for 5 times. The seeded WCFs were dipped in prepared growing solution and transferred to stainless-steel autoclave for hydrothermal heating procedure. Hydrothermal heating was performed at 220 ℃ for 24 h for synthesizing tin oxide nanorods.

The vacuum assisted rein transfer molding (VARTM) was used for preparing capacitor samples. Typically, the carbon based composite capacitor is composed with two activated carbon based electrodes and one separator. The activated carbon material electrodes have high specific area that could accumulate the electric charges. The separator prevents the electric connection between electrodes and usually filter paper, glass fiber and polypropylene membrane are used. The capability of energy storage is highly related with the available electrode surface because the electric charges in electrolyte are accumulated onto the electrode surface. In addition to that the size and concentration of electrolyte ion and electrolyte stability are also crucial factors. The glass fiber was reported as good separator material when considering both electrochemical and mechanical perspective [108]. In this process, therefore, the one layer of glass fiber was sandwiched into two prepared hybrid SnO_2-CF electrodes as separator. These three fabric layers were placed in the vacuum chamber. The copper tapes were applied to the surface of the electrodes as the current collector for electrochemical characterization. The vacuum bagging film and sealant tape were arranged over the prepared sample to create a vacuum. An inlet and outlet were employed for vacuum and resin flow to the chamber. The

60 kPa of vacuum pressure was set to the system using vacuum pump. The prepared resin was injected to the system via inlet pipe and then the chamber was maintained the vacuum state for 48 h in order to provide sufficient curing time.

The functionalized resin, in other words, solid electrolyte was prepared via mixing ionic liquid (20 %), lithium salt (10 %) and polymer resin (70 %). The lithium salt was added into the ionic liquid and stirred continuously until completely dissolved. This lithium salt and ionic liquid mixture were mixed exhaustively with polymer resin until homogeneous matrix was established. After arranging the uniformly mixed matrix, in was injected to the VARTM system and functioned as solid electrolyte. The ionic liquids are frequently utilized in conventional supercapacitors due to the large operating voltage window, high conductivity and superior thermal stability [109]. The presence of lithium salt in the ionic liquid prevents the phase separation of solid electrolyte and provides homogeneous monolithic matrix. The electrochemical performances of capacitor are enhanced as the content of the ionic liquid increasing; however, the mechanical properties of composite are decreased [110]. The electrochemical and mechanical properties of manufactured matrix generally show counterpart phenomena. Therefore, the amount of polymer resin was controlled at 70 % to minimize the deterioration of structural role. The overall procedure for fabricating structural SnO_2-capacitor is shown in Figure 4-1.

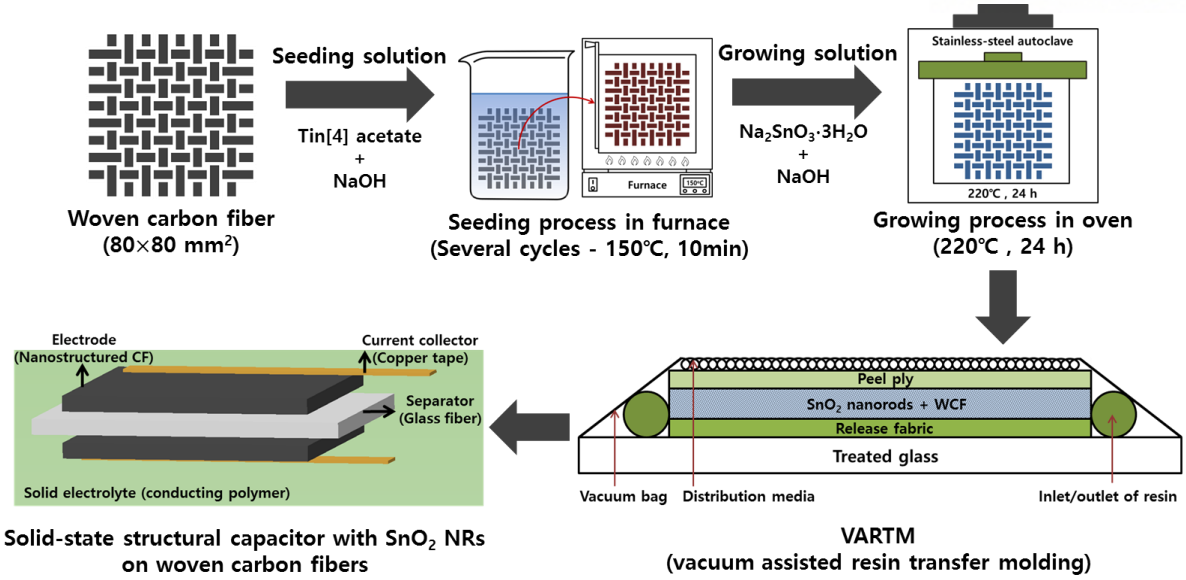

Figure 4-1. Schematic diagram for manufacturing structural SnO_2-CF capacitor.

4.2.2. Electrochemical characterization

The electrochemical performances of tin oxide modified multifunctional capacitor were depicted via two test fixtures. For identifying the performances of capacitor materials, Two- and three-electrode system are mainly considered test configurations. Three-electrode system, in other words, half-cell system usually is employed in electrochemical research and composed of a working electrode, a reference electrode and a counter electrode. In this system, the potential changes of only one electrode (i.e. working electrode) are measured, which means the voltage and charge transfer are analyzed within single electrode. The voltage potential differences are recorded with comparing to reference electrode. The counter electrode, also called auxiliary electrode, facilitates sustained current passing and hence it enables the potential of the working electrode could be measured against ascribed reference electrode. For identifying the overall performance of energy devices, the two electrode system is considered as appropriate test fixture. The analysis terminals are connected to two electrodes of packaged energy device which is generally consisted of two electrodes, one separator, electrolyte and current collector. The counter and reference electrode terminals are physically connected to each other and connected to one electrode of the test cell, and the working electrode is connected to remained electrode. The performances of whole cell which includes working electrode, electrolyte, and counter electrode are characterized through measuring the overall voltage potential differences by the current across.

The tin oxide nanords grown carbon fibers were characterized in three-electrode system as electrode for observing its performances in terms of growth concentration with multi-channel electrochemical instrument (IviumStat, Eindhoven, Netherlands). The tin oxide grown carbon fibers were characterized via cyclic voltammetry method (CV) as working electrode. Platinum coiled and saturated calomel electrodes (BAS Inc. Tokyo, Japan) were utilized as counter and reference electrode, respectively. CV experiments were performed at 0.1 V/s of scan rate in 1M KCl electrolyte. The areal capacitance of working electrode was determined by CV methods within 0 to 1 V of potential window. Prior to the test, the samples were immersed in the electrolyte and the size of immersed samples was strictly restricted with 10 mm x 10 mm square.

The solid-state structural capacitors were manufactured which consisted of two SnO_2-CF layers as electrodes, one layer of glass fiber, and functionalized resin as solid electrolyte. Each capacitor was prepared two SnO_2-CF layers which were synthesized in same growing solution. For identifying overall performances of assembled capacitors, cyclic voltammetry (CV), galvano-static charge discharge (GV), electrochemical impedance spectroscopy (EIS) measurements were performed. CV measurements were performed at 10 mV/s scan rate within 1 V of potential window for observing

current differences in terms of applied voltage. The charging and discharging capabilities were characterized via GV test with applying ± 10 mA current within same potential window. The impedance spectroscopy measurements were operated at the 0.5 V of sinusoidal voltage amplitude for identifying overall electrical resistance of capacitor samples.

4.3. Experimental results and discussions

4.3.1. BET and morphology analysis

The Brunauer-Emmett-Teller (BET) specific surface area analysis was performed in the nitrogen atmosphere using a Physisorption Analyzer (ASAP2420 Analysis, Micromeritics, Norcross, USA). The morphology of tin oxide nanorods on carbon fiber were observed using SEM (Hitachi High-Technologies Corp., Tokyo, Japan) in terms of growth concentration and BET area of SnO_2 NRs grown carbon fibers were identified as function of growth concentration. SEM results of SnO_2-WCFs are shown in Figure 4-1 and the degree of NRs growth are increasing along with SnO_2 contents increasing. All analyzed samples were represented higher BET surface area relative to bare carbon fiber (ca. 0.4088 m^2/g) [34]. The synthesized tin oxide nanostructures were increased the available surface area of interphase interaction. Although the sizes of tin oxide nanorods were increased along with molar concentration of growing solution, the 30 mM grown sample exhibited highest BET surface area (ca. 1.7953 m^2/g). As the molar concentration of tin oxide nanorods increasing, the degree of the nanorods aggregation were increased, in other words, the nanostructures were grown much denser. The pore volumes were decreased from 30 to 70 mM samples though the growth of nanorods was enhanced. These assembled growths of nanorods lowered the available surface area of nanostructures and hinders the interactions with functionalized matrix. The high surface area is beneficial for the electrodes and helps improving permeations of the electrolyte [111].

Table 4-1. BET surface area determination of SnO_2 nanorods on CF surface

	10 mM	30 mM	50 mM	70 mM
BET surface area (m^2/g)	0.7249±0.0070	1.7953±0.0155	1.6281±0.0055	1.453±0.0035
Pore volume (cm^3/g)	0.005362	0.008799	0.006324	0.006519
Pore size (nm)	29.58595	19.60475	15.53691	17.94637
Specific capacitance (F/g)	0.0337	0.2188	0.1432	0.0703

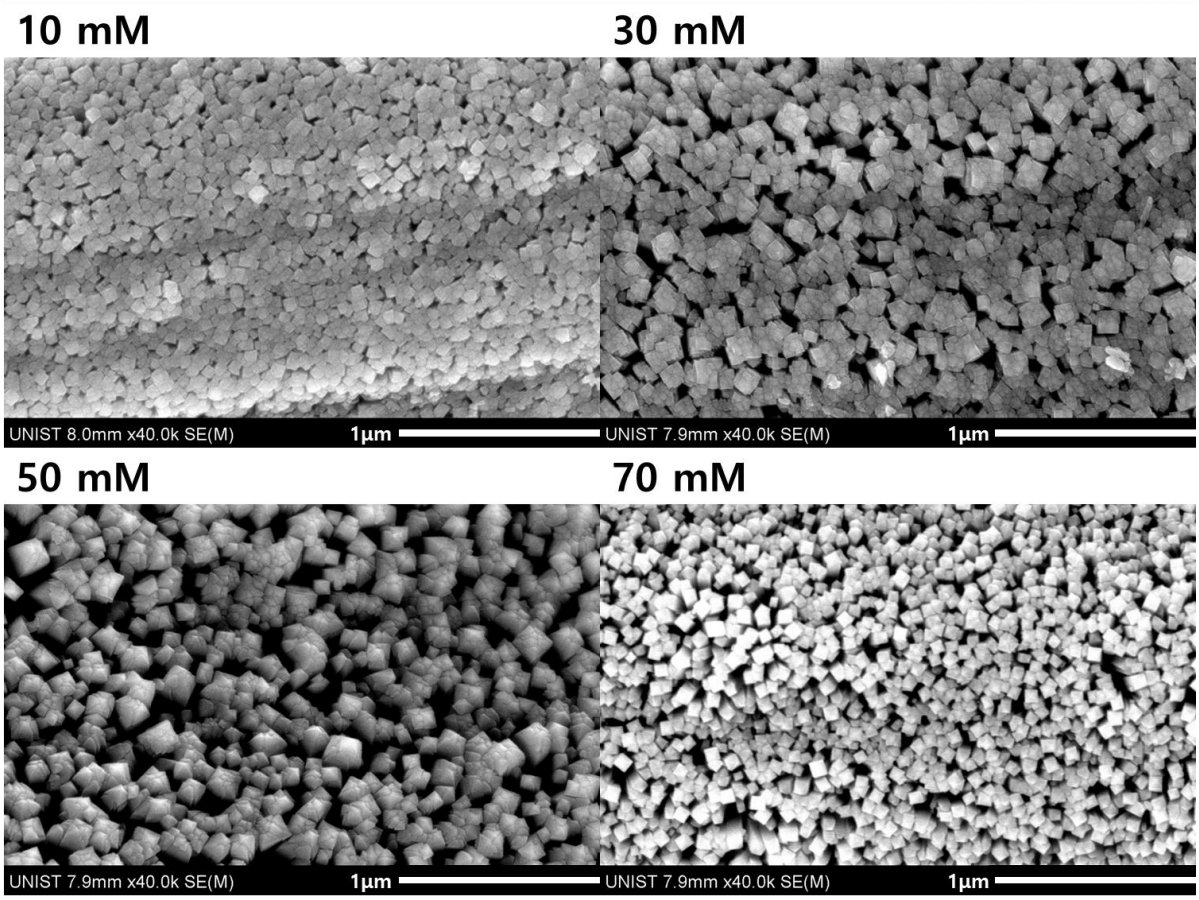

Figure 4-2. SEM images for tin oxide nanorods on carbon fiber surface

4.3.2. Cyclic voltammetry for SnO_2-WCF electrodes (three-electrode system)

The electrochemical properties of SnO_2 NRs on carbon fibers at different SnO_2 growth concentrations were evaluated through cyclic voltammetry (CV). CV is a type of potentiodynamic electrochemical measurements, in which the working electrode potential is ramped linearly versus time like linear sweep voltammetry. This is a powerful method for identifying electrode materials for electrochemical capacitor applications in the electrochemistry area. In this method, the electrodes are generally dipped in the electrolyte. Electric double layers form at the interface surfaces between electrodes and electrolyte which are accessible to ions present in the electrolyte [112]. The characterization experiments were conducted in a three-electrode system with a Pt coil as counter electrode and a SCE as reference electrode in 1M KCl solution. The electrochemical performance of SnO_2 NRs on carbon fibers were depicted at scan rate of 0.1 V/s in the potential range 0 to 1 V in terms of growth concentration of tin oxide including bare carbon fiber (Figure 4-3). The CV curves of SnO_2 NRs on carbon fibers exhibit a quasi-rectangular shape with no redox peaks which indicates that their capacitance predominantly arises from ideal behavior of electrical double layer capacitors [113]. The areal capacitance SnO_2-CF electrodes were calculated via CV tests using following equation [114]:

$$C = \frac{1}{S \cdot \nu \cdot \Delta V} \int IdV \tag{4.1}$$

where C is areal capacitance (F/cm^2), S is the area of the electrode immersed in the electrolyte, ν is the potential scan rate (V/s), ΔV is the potential window and I is the current on CV curves. In this investigation, cyclic voltammetry measurement at bare carbon fiber and various molar concentration 10, 30, 50, 70 mM performed the areal capacitance of 5.79, 8.61, 23.20, 15.73 and 10.12 mF/cm^2 respectively. The varying tendency of areal capacitance was well matched with BET analysis results. The highest areal capacitance was performed at 30 mM sample and this was larger value than reported for similar nanostructures, such as TiO2 nanotubes (3.24 mF/cm2 at 100 mV/s) [115], TiO_2 nanowires grown on carbon fibers (4.4 mF/cm2 at 10 mV/s) [113] and ZnO nanowires on flexible fibers (0.21 mF/cm2 at 100 mV/s) [116]. The higher capacitance of SnO_2-CFs can be ascribed by the two reasons: (1) high conductivity and 3-D surface of carbon fiber substrate; (2) SnO_2 nanorods were directly grown on carbon fiber and increased surface area, thus enable the enhanced interfacial charge transfer.

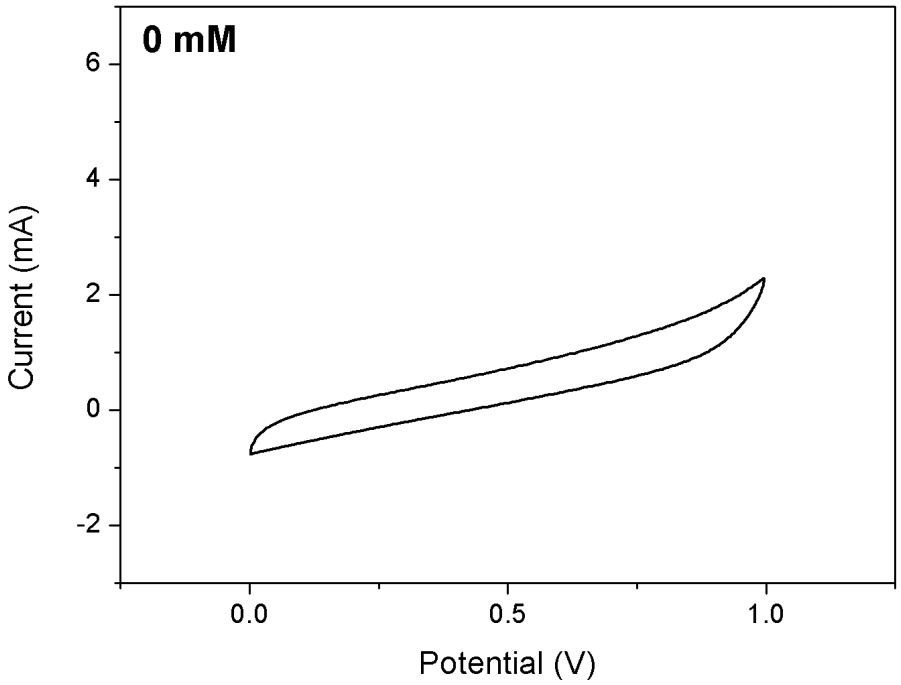

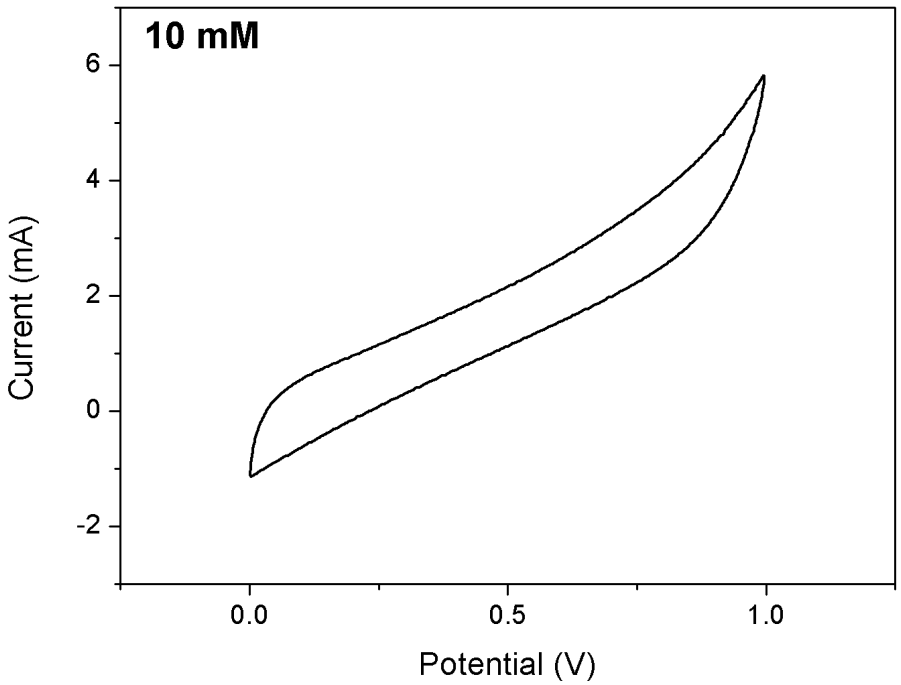

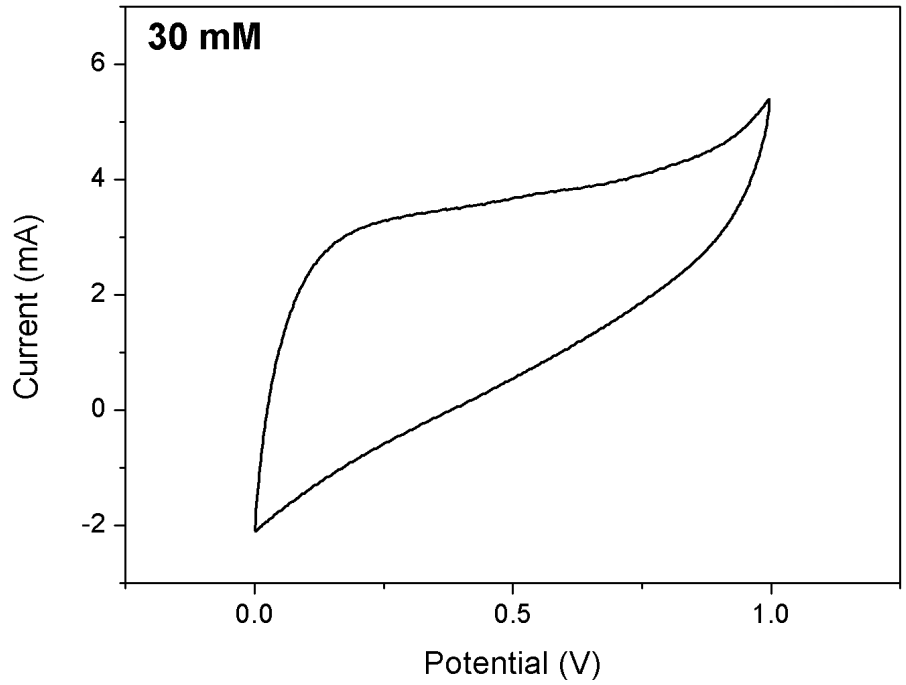

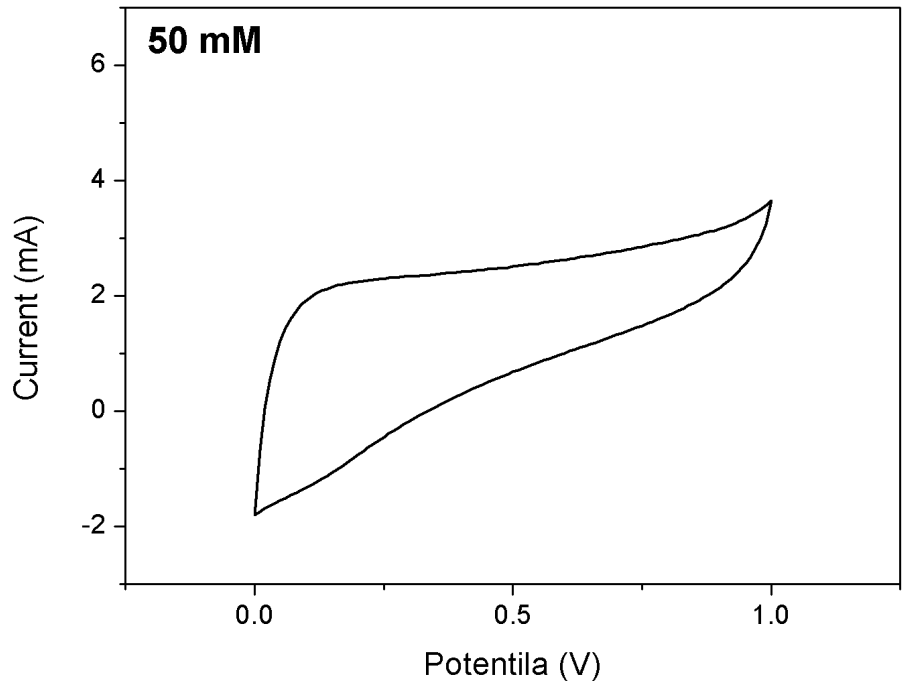

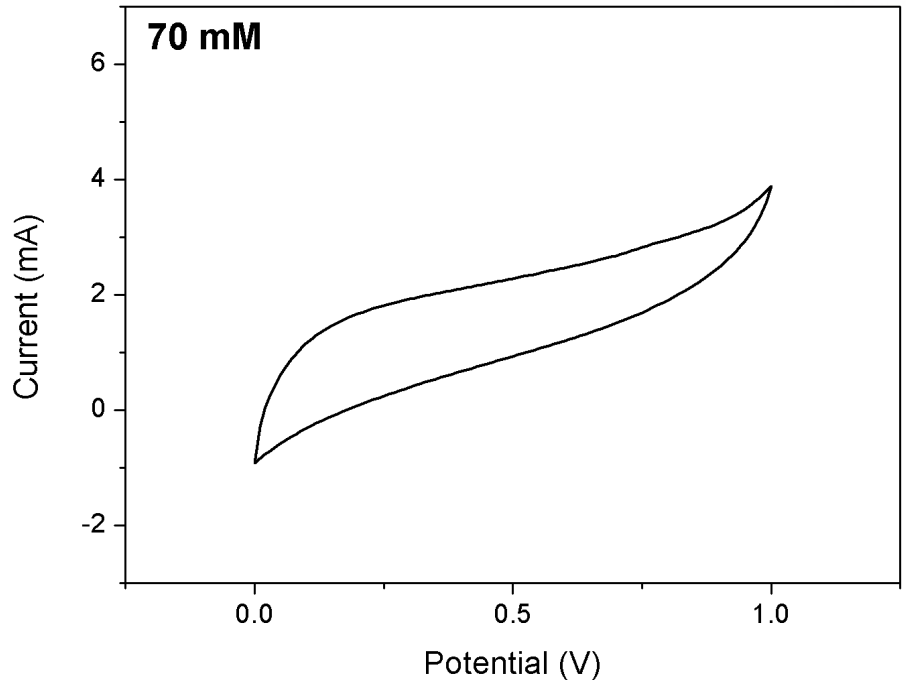

Figure 4-3. Cyclic voltammograms for SnO_2-CF electrodes

4.3.3. Electrochemical characterization for SnO_2-CF composite (two-electrode system)

The electrochemical performances of SnO_2-WCF structural capacitor was identified via CV, GV, EIS. These three analysis methods are the most frequently utilized techniques for identifying the electrochemical performance of a capacitor.

The CV analysis was performed in two electrode system in terms of growth concentration. The tests were carried out at 10 mV/s within 0-1V potential window through connected current collector. CV results of structural capacitors were shown in Figure 4-4 and these showed nearly rectangular curves which are similar with carbon fiber based capacitors [117]. As expected, the 30mM SnO_2-WCF capacitor performed largest CV curve area which represents the capability of charge storage. The pseudocapacitive redox peaks were not shown in CV curves but exhibited the double layer capacitance behaviour between the active electrode and electrolytes. The integrated area of CV curves is in good agreement with the BET area analysis result and could infer that the increased surface area facilitates electric charge storage.

The observed GV curves at current 10 mA in the voltage range 0-1 V as a function of time (s) were shown in Figure 4-5. The nearly triangular shaped GV curves demonstrates the capacitive behavior which induced by the interactions between electrodes and electrolytes. The linearity in the discharge region reaffirmed the double layer capacitance behavior without redox reactions [118]. The specific capacitance values at 0, 10, 30, 50 and 70 mM were found to be 16.94, 24.03, 141.91, 96.27, and 54.51 mF/g, respectively. These values were obtained according to following equation [119];

$$C_{cell} = \frac{I}{mdV/dt} \tag{4.2}$$

in which I is the discharge current (in A), m is the total mass of the two electrodes (in g), dV/dt is the slope of the discharge curve. The slope of the discharge curve was considered within stable operating voltage region with excluding the ohmic drop (IR drop). The initial portion of the slope in the discharge curve was considered excluding initial portion (IR drop) to avoid overestimation of the specific capacitance, dV/dt was calculated from following equation [119];

$$dV/dt = \left(V_{\max} - \frac{V_{\max}}{2} \right) / \left(T_2 - T_1 \right) \tag{4.3}$$

The high wettability that incurred by the SnO_2 nanorods increased the interlaminar contact of the electrodes with the electrolyte and enhanced the electrochemical performance. From the specific capacitance of two electrode system (C), the energy (E, in $Wh \cdot kg^{-1}$) and power (P, in $W \cdot kg^{-1}$) density of structural capacitor were estimated using the following equations [82];

$$E = \frac{1}{2} C_s V^2 \tag{4.4}$$

$$P = E / \Delta t \tag{4.5}$$

where E, C, V, P and Δt represents for energy density, specific capacitance, discharge voltage window excluding IR drop, power density and discharge time, respectively. The obtained specific capacitance, energy and power density were shown in Table 4-2. The 30 mM sample had the highest energy density, in other words, the highest amount of energy could be stored. The specific capacitance and energy density performs good agreement with BET analysis result. The increased surface area of carbon fibers enables the more electric energy could be stored through enhanced interaction within interphase region. The obtained power densities were highest in bare carbon fiber (0 mM) composite due to the light weight of the two electrodes. The electrodes weight at 0, 10, 30, 50 and 70 mM were measured to be 2.6, 3.3, 3.7, 4.4 and 4.8 g, respectively. The light weight of the bare carbon fiber (0 mM) influenced to the power density, however, the electrochemical performance as capacitor is inferior due to the low capacitance and energy density. The 30 mM sample had the second highest power density, in other words, it had the highest power density among the SnO_2 grown WCF samples. Even the contents of the tin oxide on carbon fiber surface, electrochemical performances of structural capacitors were not increased. The fiber and resin volume fractions of synthesized SnO_2-composite were also obtained by measuring the weight of SnO_2-CF samples. The weight of the tin oxide samples was measured and the density of resin, carbon fiber and SnO_2 were used for calculating volume fractions [38, 58, 78]. The fiber volume fraction at 0, 10, 30, 50 and 70 mM were calculated to be 46.16%, 43.47%, 41.23%, 44.52%, 46.95%, respectively. The fiber volume fraction result exhibits similar tendency with BET surface area results and demonstrates the higher surface area enables more resin could be infused. However, the differences of volume fraction values are located within 5%, therefore, the fiber volume fraction cannot be the critical factor for energy storage performances. From equation (2.2), the energy storage performances are mainly influenced by the specific electrode surface area and distance between two electrodes. Therefore, the thickness of synthesized SnO_2-WCF capacitor was measured and exhibited 0.830, 0.985, 0.986, 0.988 and 1.027 mm at 0, 10, 30, 50 and 70 mM samples, respectively. The differences of capacitor thickness were very low and also every capacitor was fabricated in vacuum environment. Therefore, the energy storage performance of structural capacitor is mainly controlled by specific surface area of the two electrodes.

The internal resistance of the capacitors would be increased due to the resistance of the grown tin oxide. Although the tin oxide nanostructures enhanced the surface area, the excessive amounts of tin oxide could hinder ion transfer behavior in interphase region. The internal resistance of the capacitor could be identified by Nyquist plot via measuring equivalent series resistance (ESR).

The electrochemical impedance spectroscopy measurements were conducted with the 0.5 V of the sinusoidal voltage in two electrode system. EIS is a useful technique complementary to galvanostatic charge discharge measurements that gives more information on the electrochemical frequency behavior of the system. The EIS data were presented via Nyquist plots and shown in Figure 4-6. The high frequency resistor-capacitor (RC) loops or semicircles were not depicted which indicates a good electrode contact [120]. The vertical lines close to 90 degree demonstrates the ideal capacitive nature of the carbon fiber electrodes [87]. The high performance capacitor demands large values of specific capacitance and low values of ESR [121]. The 30 mM sample performed the lowest ESR and overall difference tendency of SnO_2-WCF capacitors was well matched with specific capacitance and BET results. The SnO_2-WCF composite revealed the poor ESR relative to conventional supercapacitors [122]. The poor ionic conductivity of the matrix could be one reason though the presence of ionic liquid and lithium salt. Aqueous electrolytes such as KCl and H_2SO generally have smaller ion size and lower ESR relative to ionic liquid but lower breakage voltage. The ionic liquid could be operated under high voltage up to 4.3-4.5 V [123].

Table 4-2. Overall electrochemical energy storage perforemances and ESR for structural SnO_2-CF capacitors.

	Specific capacitance (mF/g)	Energy density (10^{-3} Wh/kg)	Power density (W/kg)	ESR (R_s) (Ω)
0mM	21.78	1.54	1.63	810.0
10mM	30.39	2.05	1.06	774.7
30mM	147.53	15.06	1.16	681.7
50mM	100.64	8.04	0.86	699.1
70mM	56.78	4.25	0.76	726.0

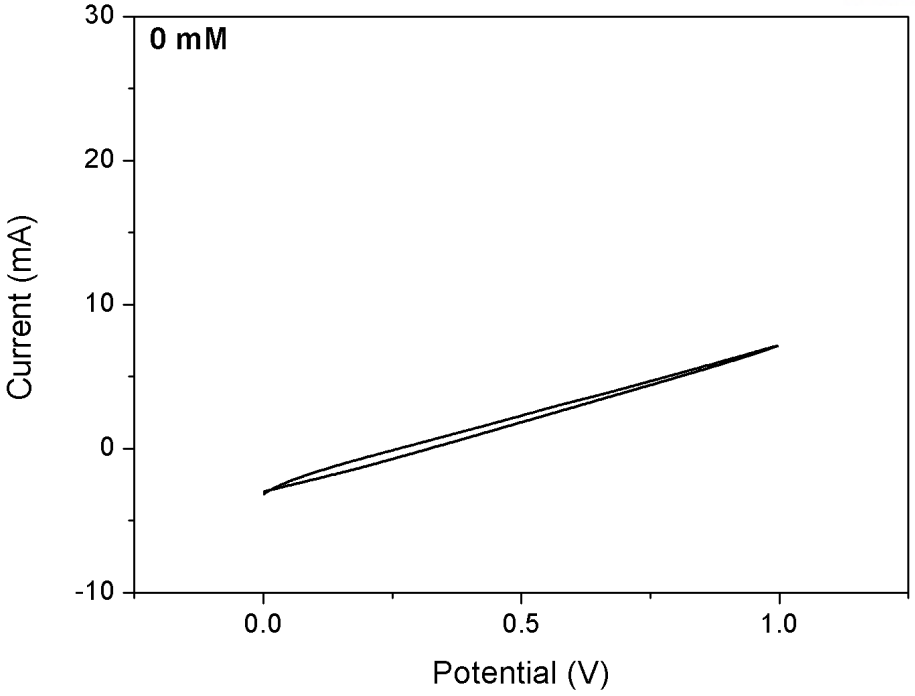

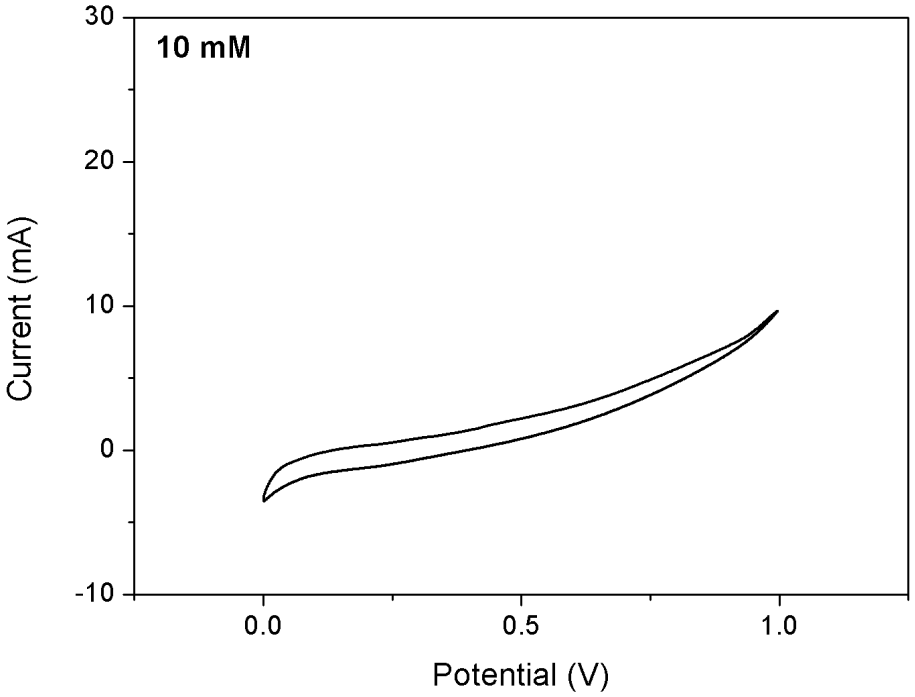

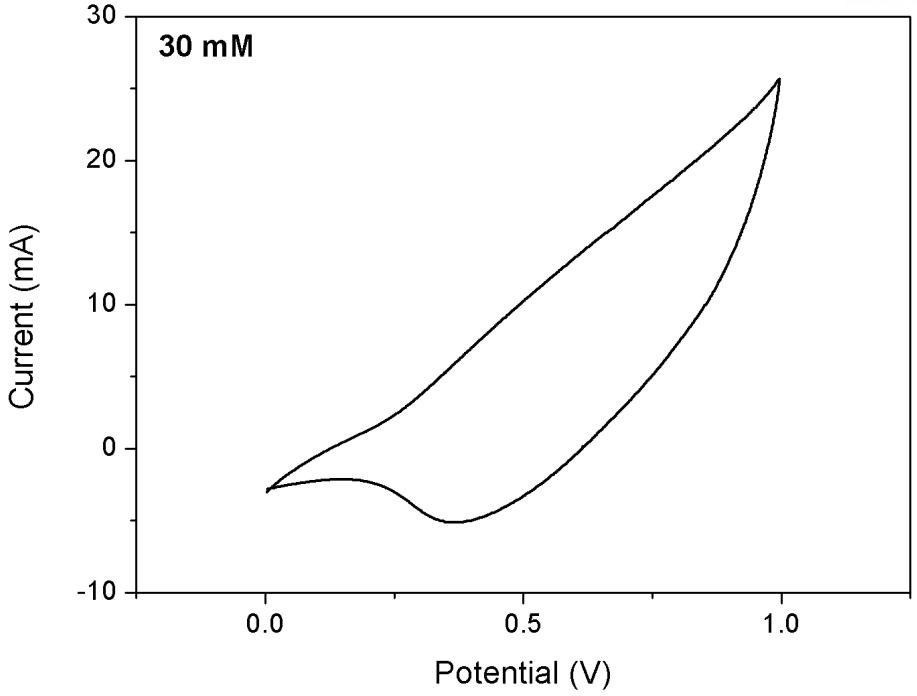

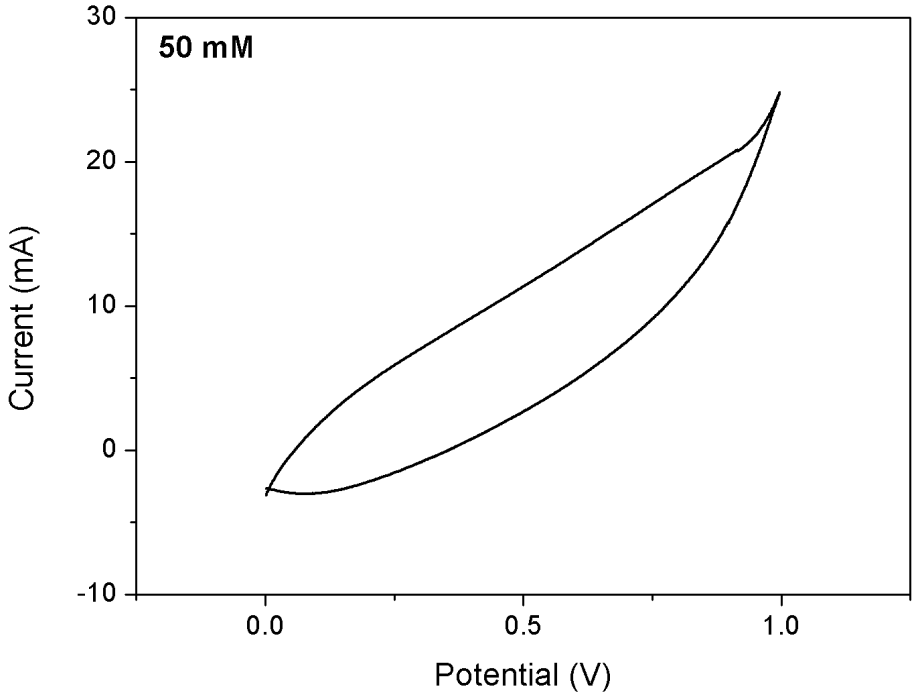

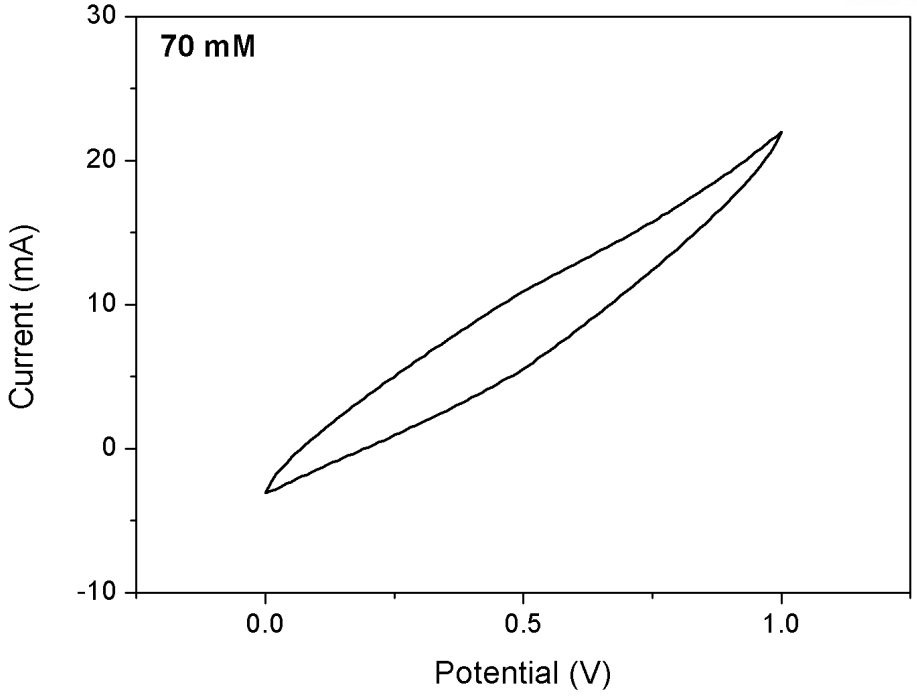

Figure 4-4. Cyclic voltammograms for structural SnO_2-CF capacitor

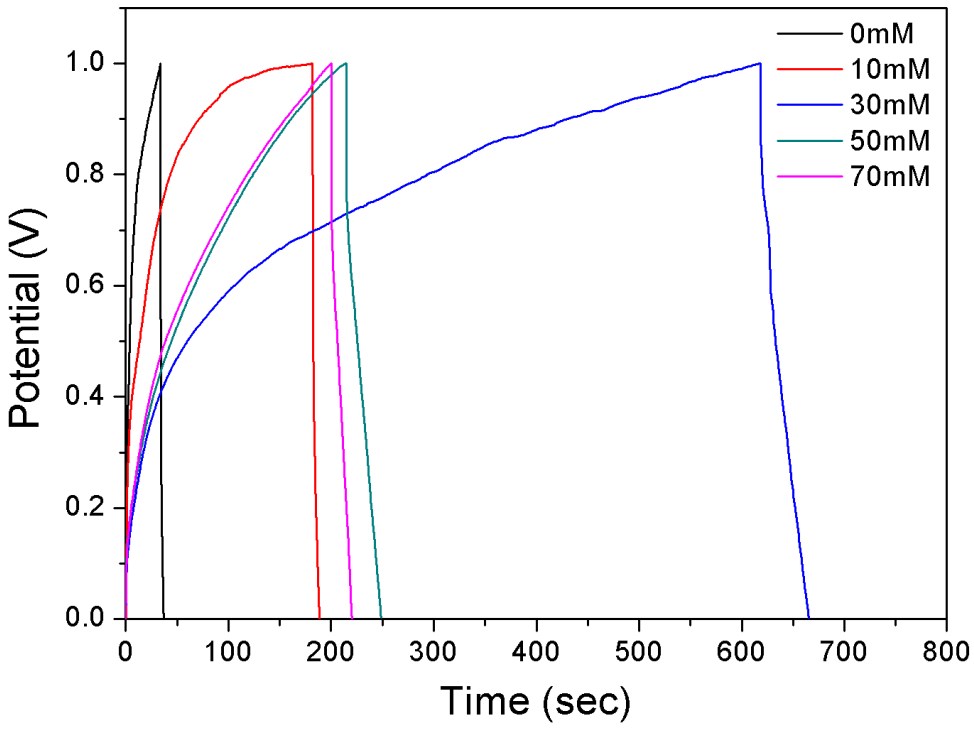

Figure 4-5. Galvanostatic charge discharge curves for structural SnO_2-CF capacitors.

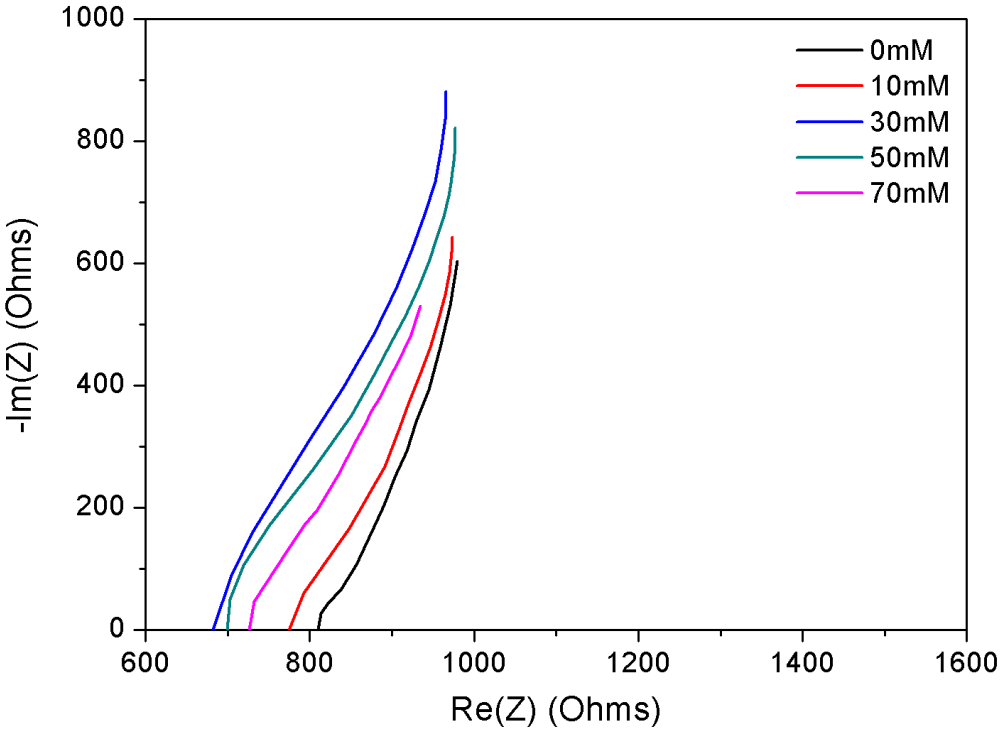

Figure 4-6. Nyquist plots for structural SnO_2-CF capacitors.

5. Conclusions

In the following section, the mechanical and energy storage performances were compared with other metal oxide nanomaterials such as ZnO and CuO. Both, metal oxide materials are also frequently used due to its extensive applications for sensors and energy storage/harvesting devices [35-37, 39-41].

In mechanical property comparison, the ZnO and CuO nanostructures were synthesized using same hydrothermal methods with one-dimensional nanorod morphology. These synthesized nanostructures were worked as secondary reinforcements within interphase region and compared in terms of molar concentration differences of growth solution.

The electrochemical properties were also characterized with ZnO and CuO nanorods which synthesized by two step hydrothermal methods. The 30 mM concentration sample was selected and compared for observing energy storage performance as structural capacitor form. The operating potentials of each nanomaterial are different due to its different electrochemical potentials. The ZnO is generally analyzed under 0.6 V potential amplitude as electrode material [124-126] and CuO is studied under 0.5 V of potential window [127-129]. Therefore, the electrochemical performances of SnO_2, ZnO and CuO were evaluated within -0.5 to 0.5 V of potential window for the comparison. The pseudocapacitive effect which employed by redox reaction was not involved in these tests.

5.1. Mechanical property comparison with ZnO, CuO

For comparing the improvements of mechanical performances, the previous mechanical test results of ZnO- and CuO-CF composite were utilized [33, 34]. The ZnO and CuO nanorods were synthesized by same hydrothermal methods and the effects of molar concentration were considered. Impact and tensile test results were referred to compare the impact absorbed energy, tensile strength, and modulus. The increased percent of impact resistance and stiffness were obtained to compare the effectiveness of whisker. The impact and tensile test results are depicted in Figure 5-1 and 5-2.

These three metal oxide nanostructures were worked as the secondary reinforcements in composite and exhibited different mechanical properties which were attributed by different affinity of functional groups and distinctive morphologies. In addition, the nanostructured density of metal oxides involves interfacial states between fibers and matrix. Among the three metal oxides, the tin oxide presented the highest stiffness of composite and this result attributes well matched results in basic property comparisons at Table 1-1. Especially, the modulus was drastically enhanced as molar concentration increasing relative to other samples. The impact response properties were best at ZnO composite, however; improvement of tin oxide was better than CuO. In addition, the tin oxide nanorods were demonstrated superior impact resistance and strength as growth concentration increasing.

(a)

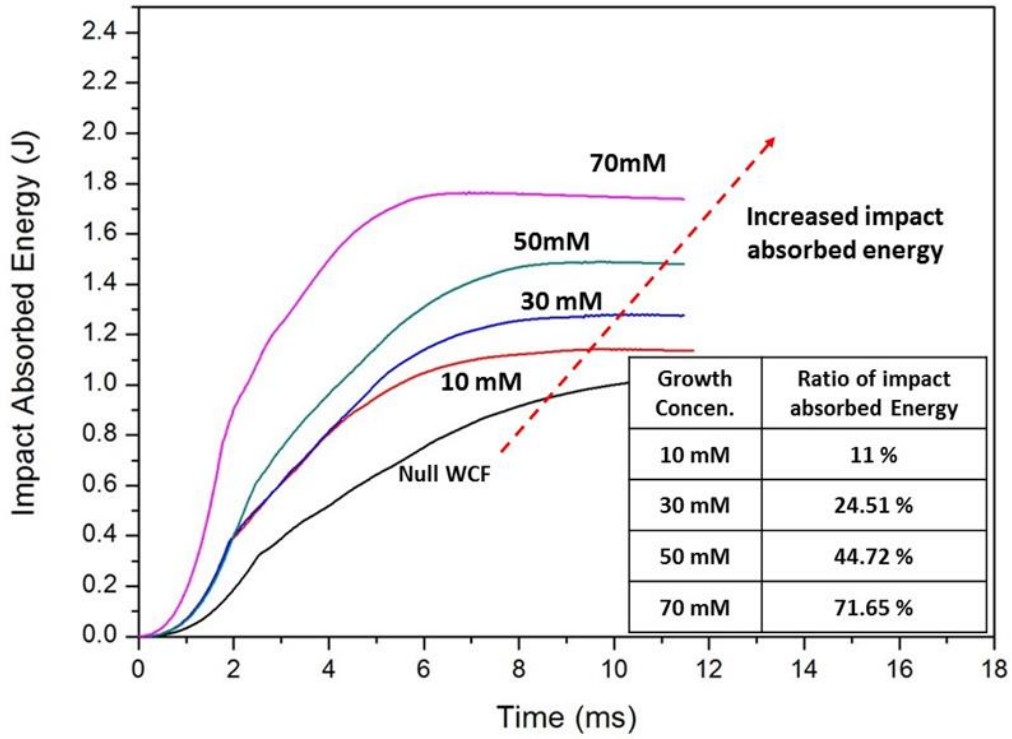

(b)

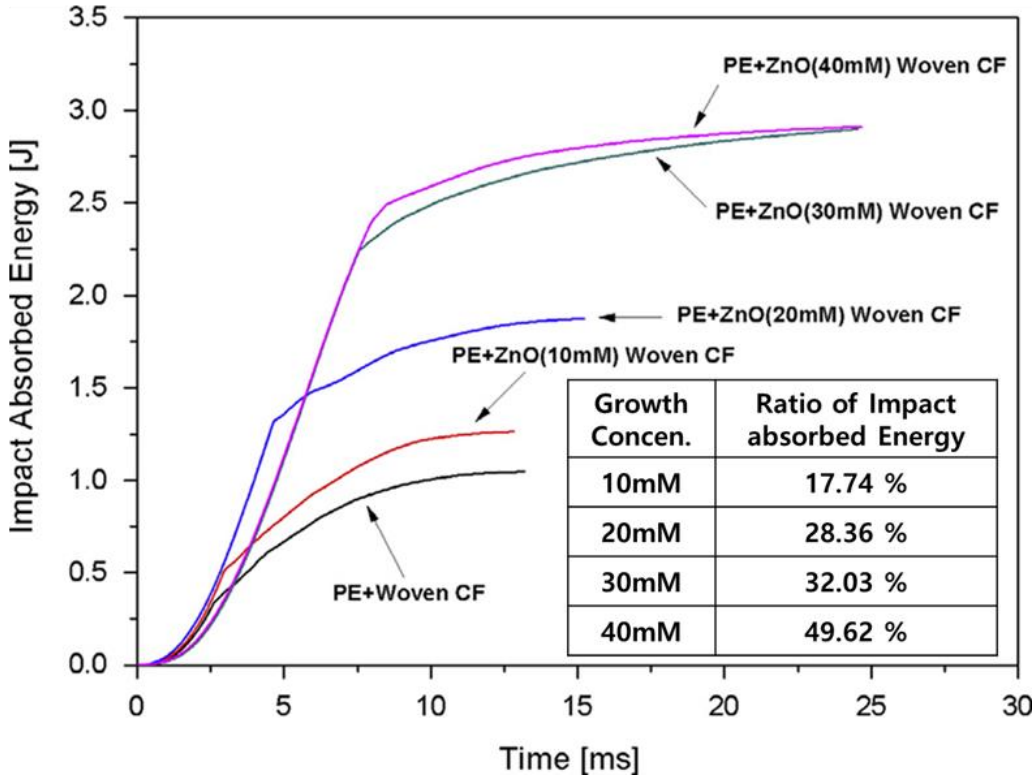

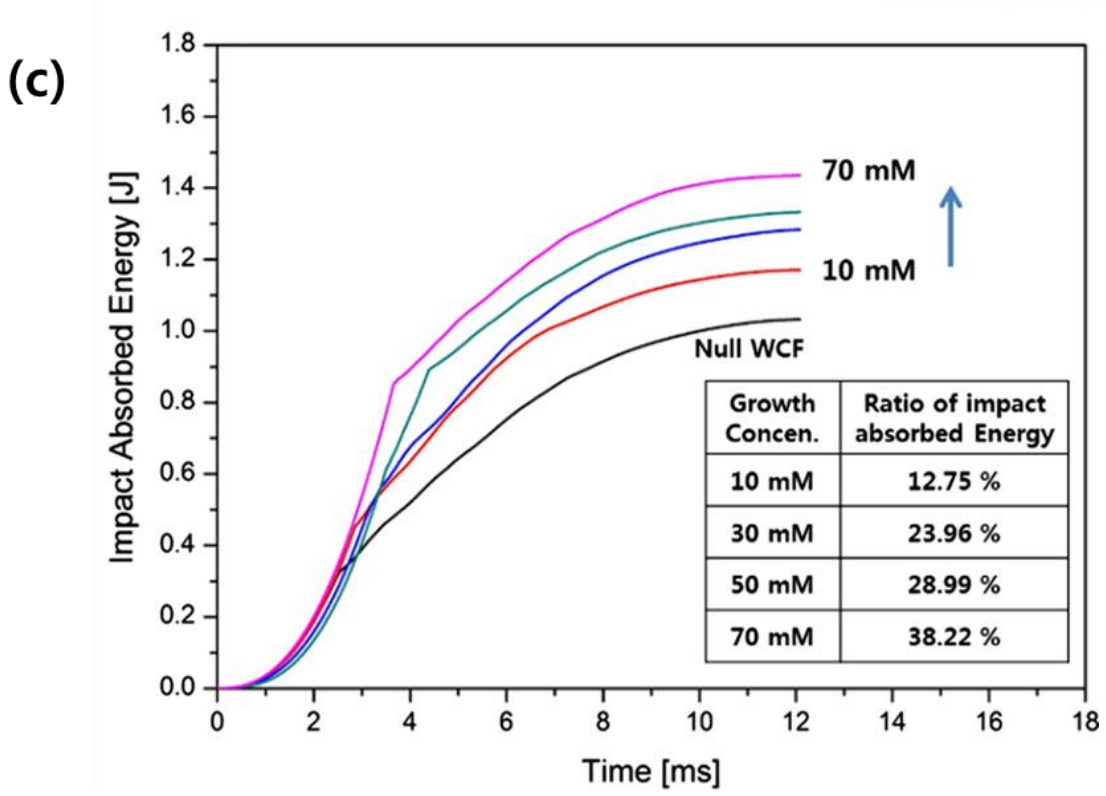

Figure 5-1. Impact test graphs for (a) SnO_2, (b) ZnO, and (c) CuO.

(A)

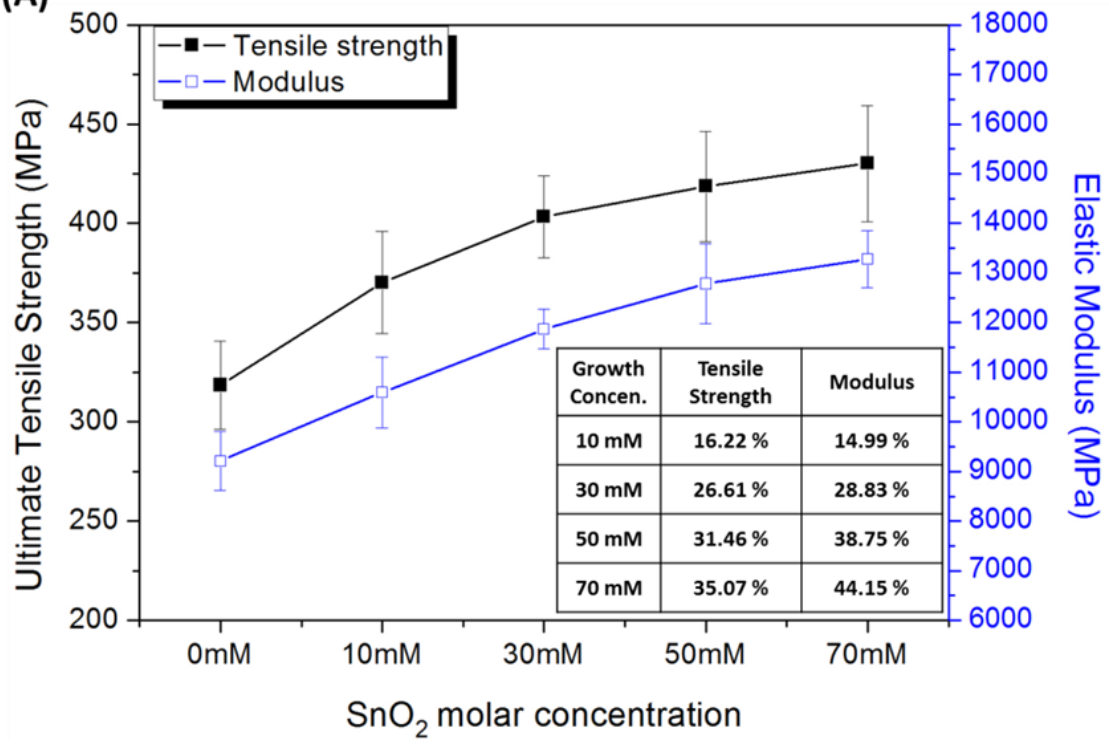

Growth Concen.	Tensile Strength	Modulus
10 mM	16.22 %	14.99 %
30 mM	26.61 %	28.83 %
50 mM	31.46 %	38.75 %
70 mM	35.07 %	44.15 %

(b)

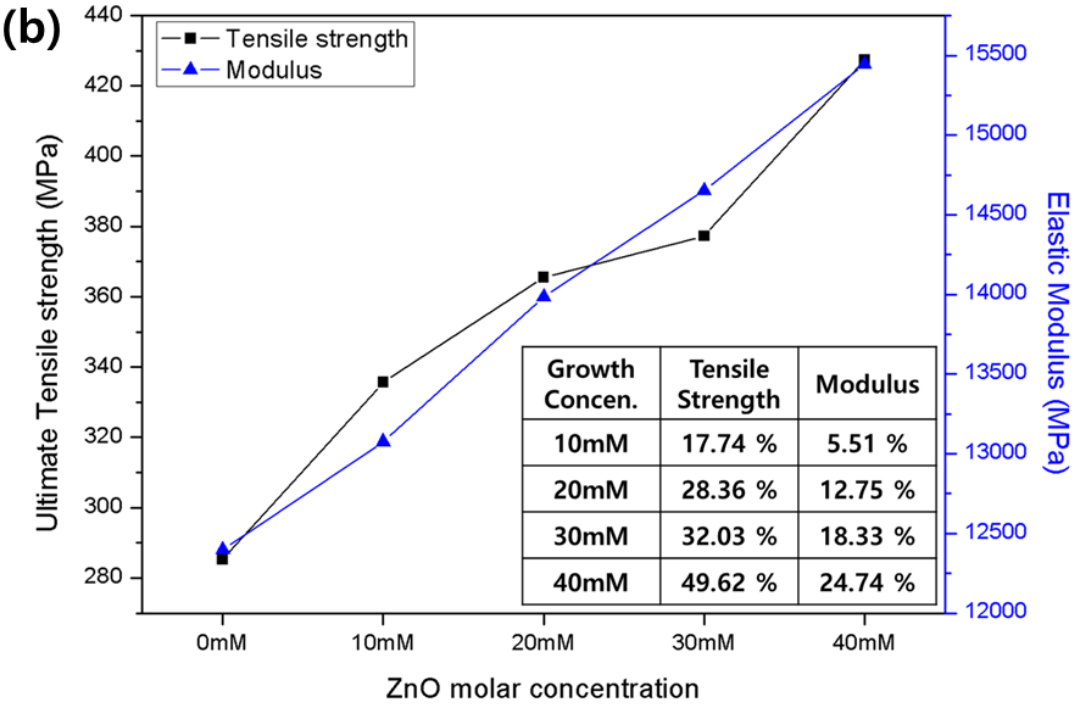

Growth Concen.	Tensile Strength	Modulus
10mM	17.74 %	5.51 %
20mM	28.36 %	12.75 %
30mM	32.03 %	18.33 %
40mM	49.62 %	24.74 %

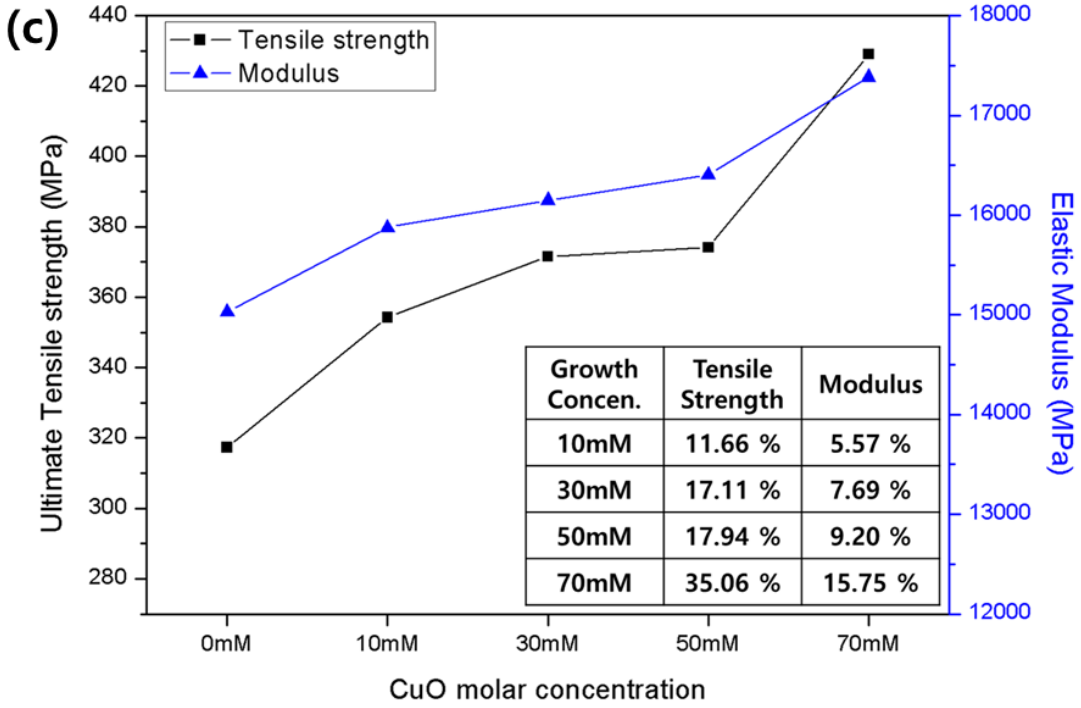

Growth Concen.	Tensile Strength	Modulus
10mM	11.66 %	5.57 %
30mM	17.11 %	7.69 %
50mM	17.94 %	9.20 %
70mM	35.06 %	15.75 %

Figure 5-2. Tensile test graphs for (a) SnO_2, (b) ZnO, and (c) CuO

5.2. Electrochemical energy storage performance comparison with ZnO and CuO

As mentioned before the operating potential ranges were set between -0.5 to 0.5 V and 30 mM of growth concentration was selected for energy storage performance comparison. The electrochemical analysis conditions were same; 10 mV/s of scan rate for CV, 10 mA current for GV and 0.5 V of sinusoidal voltage amplitude for EIS. ZnO and CuO nanostructured CF were fabricated by same hydrothermal process and structures of multifunctional structural capacitors were equally developed via VARTM. The synthesis process of ZnO and CuO was referred from previous reports [33, 34].

In Figure 5-3, the compared CV, GV and EIS results are presented and specific capacitance, energy and power density, and ESR are summarized in Table 5-1. Based on CV curves, the redox reactions were excluded in all metal oxides and exhibited the electric double layer behavior. Even the highest theoretical capacitance of ZnO, the energy storage performances were inferior. The low performances of ZnO were attributed by high resistance and poor intrinsic properties for electrochemical energy storage functions [45]. The ZnO sample presented shortest charging time in GV results and this demonstrates the low energy storage capability. The CuO sample was performed longer charging time than ZnO, however; specific capacitance was lower than SnO_2 due to the small value of discharge slope. Although the theoretical capacitance was lowest among the metal oxides, the relatively higher dielectric constants could be attributed the higher specific capacitance than ZnO. Among them, the SnO_2 nanorods presented best capacitive results. All the summarized values in Table 5-1 were indicated that the best energy storage performances of SnO_2-CF structural capacitor. These superior results were carried out due to the high theoretical capacitance, enhanced accessible surface area for electric charge, and lowest internal resistance (ESR) of fabricated cell. In addition, tin oxide can be operated at higher voltage amplitude about 1 V which advantageous characteristic for energy storage applications.

Table 5-1. Electrochemical performances of CuO, ZnO, and SnO_2

Metal oxide	Specific capacitance (mF/g)	Energy density (10^{-3} Wh/kg)	Power density (W/kg)	ESR (R_s) (Ω)
CuO	6.42	0.63	0.50	689.6
ZnO	2.73	0.27	0.38	720.1
SnO_2	17.78	2.18	1.46	681.7

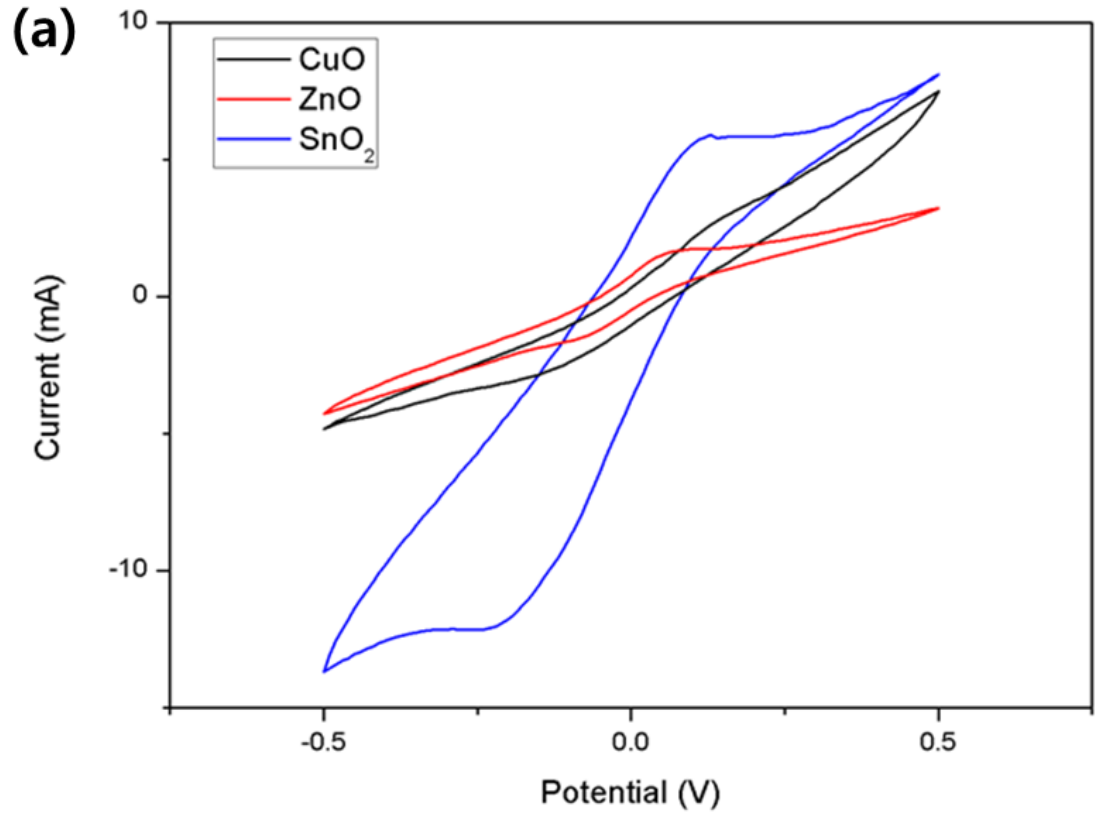

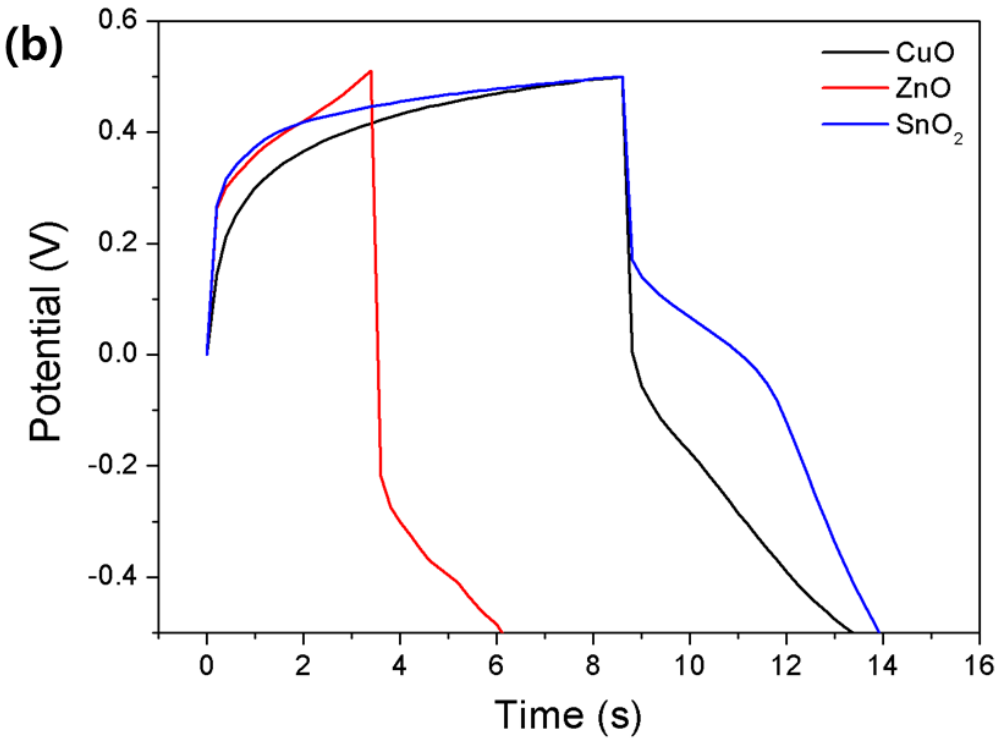

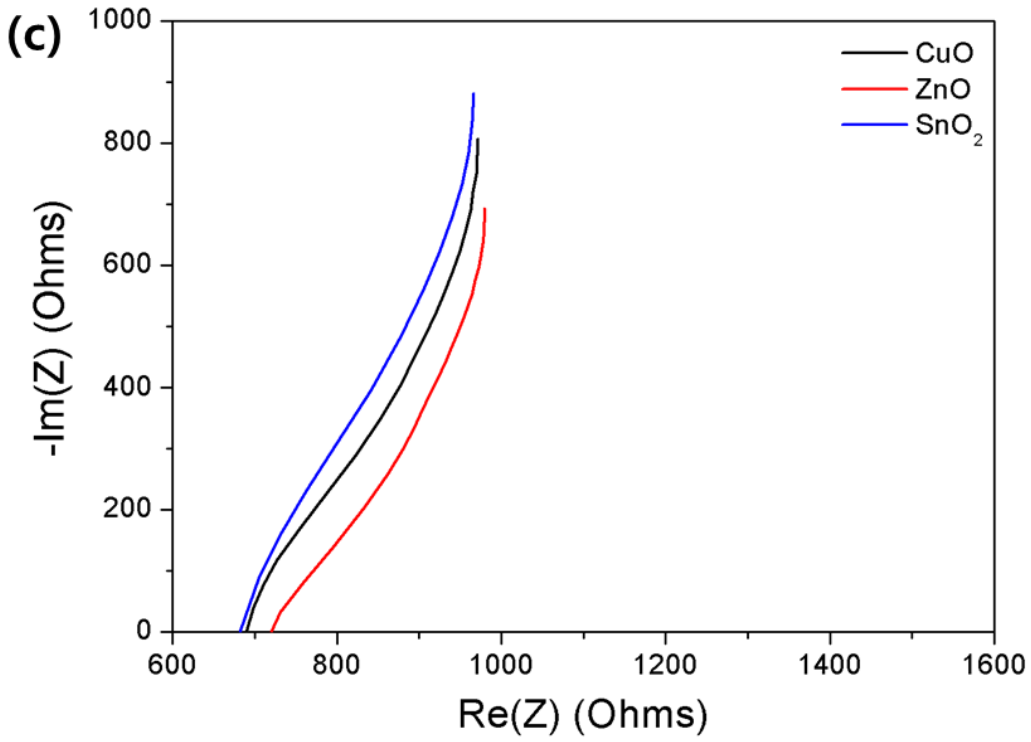

Figure 5-3. Electrochemical analysis results for CuO, ZnO, and SnO_2, (a) Cyclic voltammogram, (b) Galvanostatic charge discharge graph, and (c) Nyquist plot

5.3. Summary

In this thesis, the tin oxide nanorods on carbon fiber surfaces were focused and studied for highlighting mechanical and electrochemical energy storage properties. The tin oxide nanostructures were performed as the secondary reinforcements within interlaminar region. SnO_2 nanostrucutured CFRPs were finalized by mechanical and electrochemical tests to evaluate the role of tin oxide whiskerization, and the improved mechanical and energy storage performances were achieved. It was disclosed that the interfacial states between fibers and matrix critically influences to overall performances of composites and thus the SnO_2 nanorods were successfully functioned as the secondary reinforcement.

SnO_2 nanorods were successfully synthesized on CF surfaces via two step hydrothermal method with different growth concentrations. The nanostructures were anisotropically grown by self-assembly mechanism at high pH level of growth solution. SEM, XRD, XPS, and BET analysis were utilized for identifying the morphologies and structures of tin oxide. The uniformly synthesized nanostructures and no other contaminants were discovered on CF surface except SnO_2 based on SEM and XRD results. In addition, the well attached nanorods on CF surfaces were identified by XPS study and enhanced surface area was achieved. According to BET analysis, the 30 mM of growth solution sample exhibited the highest surface area and the pore volume was identified that closely grown SnO_2 structures at higher growth concentration.

According to the mechanical and electrochemical experiments, it was revealed that tin oxide nanorods were improved the performances of CFRP composite. In impact and tensile tests, enhanced impact absorbed energy (71.65 %), ultimate tensile strength (35.07 %), in-plane shear strength (49.07%), and elastic modulus (44.15%) were exhibited in SnO_2 fabricated composite. The infacial interactions between fibers and matrix were increased due to the role of the SnO_2 nanorods as whiskers. Enhanced surface area of CF surface and surface functional groups on nanostructures were achieved increased load transfer from external forces and improved crack resistance from impact. Synthesized SnO_2 reinforced the overall CFRP as secondary reinforcements and achieved the enhanced structural functions. The energy storage functions as multifunctional material were evaluated by electrochemical test with developed SnO_2-CF structural capacitors. The experimental conditions in CV, GV and EIS were set for appropriate performance identification. As expected from referred literatures, it was disclosed that the surface area of electrode is crucially affects to the energy storage performances. The surface area of electrode was highest in 30 mM sample and thus the improved specific capacitance (147.53 mF/g), energy density (15.06 mWh/kg), and power density

(1.16 W/kg) were exhibited. The enhanced accessible surface area for electric charge was achieved by 1-D aligned nanostructures, therefore; more capabilities for energy storage can be achieved. The multifunctionality of SnO_2 reinforced CFRP was characterized in terms of mechanical and energy storage functions and tin oxide nanomaterials were highly considered for achieving enhanced performances of composite.

5.4. Future works

Multifunctionality of the SnO_2-CF composite was exhibited in this thesis. Both the enhanced mechanical properties and energy storage performances were achieved by tin oxide nanorods on CF surfaces. However, the energy storage performances of manufactured structural capacitors were relatively lower than other typical energy devices due to its structural limitations for using solid polymer resin and high resistance of overall cell system. There are several potentials for improving performances of multifunctional capacitors. One is the modifying the solid electrolyte resin. The existence of polymer resin provides the structural functions on composite, but it also lowers the contents of ions and degrades the role of electrolyte. Generally, the mechanical and energy storage performances present the cross-cutting phenomena, therefore; finding the optimized condition is really challenging which satisfies both structural and energy storage functions. However, the rewards of developing such optimized composite are enormous, offering huge advantages for reducing volume and weight of system.

6. References

[1] J. B. Donnet and RC Bansal., Carbon Fibers, New York: Marcel Dekker, Inc., (1990).

[2] Chand S., Review carbon fibers for composites, Journal of Materials Science 35 (2000) 1303-1313.

[3] Weitzsacker L, Ming X and Drzal L. T., Analysis to investigate fiber/matrix chemical interactions in carbon fiber reinforced composites, Surf Interface Anal 25 (1997) 53-63.

[4] Jacobasch H. J. et al., Comparison of surface chemical methods for characterizing carbon fiber epoxy resin composites, Compos Interfaces 3 (1996) 293-320.

[5] Ibarra L., Macias A., and Palma E., Stress strain and stress relaxation in oxidated short carbon fiber thermoplastic elastomer composites, J Appl Polym Sci 61 (1996) 2447-2454.

[6] Delamar M. et al., Modification of carbon fibers surfaces by electrochemical reduction of aryl diazonium salts application to carbon epoxy composites, Carbon 35 (1997) 801-807.

[7] Hiroshi A. et al., Effect of pyrocarbon precoating on the mechanical properties of CVI carbon fiber SiC composites, J Nucl Sci Tech 32 (1995) 369-371.

[8] Tiwari S. and Bijwe J., Surface treatment of carbon fibers - a review, Procedia Technology 14 (2014) 505-512.

[9] Yang B. X., et al. Mechanical reinforcement of polyethylene using polyethylene-grafted multiwalled carbon nanotubes, Adv Funct Mater 17 (2007) 2062-2069.

[10] Huang H. et al., Chem and G. Shen, Metal oxide nanowire transistors, J. Mater. Chem. 22 (2012) 13428-13445.

[11] Kolmakov A. et al., Detection of CO and O-2 using tin oxide nanowire sensors, Adv. Mater 15(12) (2003) 997.

[12] Sugimoto H., Tsukube H. and Tanaka K., Immobilization of a high-valent rhenium complex on an indium-doped tin-oxide electrode: enhanced catalytic activity of a trans-dioxorhenium(v) complex in electrochemical oxidation of alcohols, Eur. J. Inorg. Chem. 23 (2004) 4550-4553.

[13] Hossain M. A. et al., Carrier generation and collection in CdS/CdSe-Sensitized SnO_2 solar cells exhibiting unprecedented photocurrent densities, Acs Nano 5 (4) (2011) 3172-3181.

[14] Kuo S. L. and Wu N. L., Composite Supercapacitor Containing Tin Oxide and Electroplated Ruthenium Oxide, Electrochem. Solid-State Lett. 6 (2003) A85-A87.

[15] Quirk J. and Harman C. G., Properties of a Tin Oxide-Base Ceramic body, Journal of the American Ceramic Society 37 (2006) 24-26.

[16] Zhu X. et al., Reduced graphene oxide/tin oxide composite as an enhanced anode material for lithium ion batteries prepared by homogenous coprecipitation, J. Power Sources 196 (2011) 6473-6477.

[17] Maddalena A. et al., Electrical conductivity of tin oxide films prepared by the sol-gel method, Journal of Non-Crystalline Solids 121 (1990) 365-369.

[18] Ghoshtagore R. N., Mechanism of CVD thin film SnO2 formation, Journal of the Electrochemical Society 125 (1978) 110-117.

[19] Ma L. A. and Guo T. L., Synthesis and field emission properties of needle-shaped SnO2 nanostructures with rectangular cross-section, Mater Lett. 63 (2009) 295-297.

[20] Cheng G. et al., Solvothermal controlled growth of Zn-doped SnO_2 branched nanorod clusters, J. Cryst. Growth 309 (2007) 53-59

[21] Wang Y.L. et al., Hydrothermal preparation and photoelectrochemical performance of size-controlled SnO_2 nanorod arrays, Crystengcomm 12 (2010) 4024-4027.

[22] Sain S. et al., Structural interpretation of SnO_2 nanocrystals of different morphologies synthesized by microwave irradiation and hydrothermal methods, CrystEngComm 16 (2014) 1079-1090.

[23] Guo J. et al., Three-dimensional SnO_2 microstructures assembled by porous nanosheets and their superior performance for gas sensing, Powder Technol. 250 (2013) 40-45.

[24] Zhao K. et al., Novel multi-layered SnO_2 nanoarray: self-sustained hydrothermal synthesis, structure, morphology dependence and growth mechanism, CrystEngComm 17 (2015) 2030-2040.

[25] Thomas J. P. and Qidwai M. A., Mechanical design and performance of composite multifunctional materials, Acta Mater 52 (2004) 2155-2164.

[26] Friedrich K., Fakirov S. and Zhang Z., Polymer composites: from nano- to macro-scale, New York, USA: Springer Science & Business Media, Inc., (2005).

[27] Luo X. and Chung D. D. L., Carbon-fiber/polymer-matrix composites as capacitors, Compos Sci Technol 61 (2001) 885-888.

[28] Thomas J. P. et al., Multifunctional structure-battery composites for marine systems, J Compos Mater 47 (2013) 5-26.

[29] Shirshova N. et al., Greenhalgh ES, Curtis PT, et al. Structural composite supercapacitors, Composites Part A 46 (2013) 96-107.

[30] Qian H. et al., Carbon nanotube grafted carbon fibres: a study of wetting and fibre fragmentation, Composites Part A 41 (2010) 1107-1114.

[31] Qian H. et al., Multifunctional structural supercapacitor composites based on carbon aerogel modified high performance carbon fiber fabric, ACS Appl Mater Interfaces 5 (2013) 6113-6122.

[32] Wetzel E. D., Reducing weight: Multifunctional composites integrate power, communications, and structure, AMPTIAC Q 8(4) (2004) 91-95.

[33] Kong K. et al., Processing and mechanical characterization of ZnO/polyester woven carbon-fiber composites with different ZnO concentrations, Composites: Part A 55 (2013) 152-160.

[34] Kong K. et al., Effect of CuO nanostructure morphology on the mechanical properties of CuO/woven carbon fiber/vinyl ester composite, Composites: Part A 78 (2015) 48-59.

[35] Mai WJ, Liang ZW, Zhang L, Yu X, Liu PY, Zhu HM, et al. Strain sensing mechanism of the fabricated ZnO nanowire-polymer composite strain sensors. Chem Phys Lett 2012;538:99–101.

[36] Peng WB, He YN, Wen CB, Ma K. Surface acoustic wave ultraviolet detector based on zinc oxide nanowire sensing layer. Sens Actuat A – Phys 2012;184:34–40.

[37] Wang ZL, Song JH. Piezoelectric nanogenerators based on zinc oxide nanowire arrays. Science 2006;312(5771):242–6.

[38] O. Madelung, Semiconductors: data handbook, Springer, Berlin (2004).

[39] Hsueh HT, Hsueh TJ, Chang SJ, Tsai TY, Hung FY, Chang SP, et al. CuO-nanowire field emitter prepared on glass substrate. IEEE Trans Nanotechnol 2011;10(5):1161–5.

[40] Kwon JD, Kwon SH, Jung TH, Nam KS, Chung KB, Kim DH, et al. Controlled growth and properties of p-type cuprous oxide films by plasma-enhanced atomic layer deposition at low temperature. Appl Surf Sci 2013;285:373–9.

[41] Yang Z., Wang D., Li F., Liu D., Wang P., Li X. et al. Facile synthesis of CuO nanorod for lithium storage application. Mater Lett 2013;90:4–7.

[42] A. Punnoose, H. Magnone, M.S. Seehra, J. Bonevich, Bulk to nanoscale magnetism and exchange bias in CuO nanoparticles, Physical Review B, 64 (2001) 174420.

[43] X. Zhang, Y.-G. Guo, W.-M. Liu, J.-C. Hao, CuO three-dimensional flowerlike nanostructures: Controlled synthesis and characterization, Journal of Applied Physics, 103 (2008) 114304.

[44] G. Filipič, U. Cvelbar, Copper oxide nanowires: a review of growth, Nanotechnology, 23 (2012) 194001.

[45] Zeng H. et al., Synthesis, optical and electrochemical properties of ZnO nanowires/graphene oxide heterostructures, Nanoscale Res Lett. 8(1) (2013) 133.

[46] Maki-Jaskari MA and Rantala TT, Possible structures of nonstoichiometric tin oxide: the composition Sn2O3, Modeling Simul. Mater. Sci. Eng. 12 (2004) 33-41.

[47] Batzill M. and Diebold U., The surface and materials science of tin oxide, Progress in Surface Science 79 (2005) 47-154.

[48] Schleife A. et al., Tin dioxide from first principles: Quasiparticle electronic states and optical properties, Phys. Rev. B 83 (2011) 035116.

[49] Chen R. et al., Characteristics of ultraviolet photoluminescence from high quality tin oxide nanowires, Appl. Phys. Lett. 95 (2009) 061908.

[50] Liu L. et al., Superior cycle performance and high reversible capacity of SnO2/graphene composite as an anode material for lithium-ion batteries, Scientific Reports 5 (2015) 9055.

[51] Zhang W. et al., ZnO nanocrystals as anode electrodes for lithium-ion batteries, Journal of Nanomaterials (2016) 8056302.

[52] Wu D. and Zhang Q., LDSA+U study of cupric oxide: Electronic structure and native point defects, Phys. Rev. B 73 (2006) 235206.

[53] Chen K., Xue D. and Komarneni S., Beyond theoretical capacitor in Cu-based integrated anode: Insight into the structural evolution of CuO, J. Power Sources 275 (2015) 136-143.

[54] Ashby M. F. and Brechet Y. J. M., Designing hydric materials, Acta Materialia 51 (2003) 5801-5821.

[55] Savage G., Formula 1 Composite Engineering, Energineering Failure Analysis (2010) 92-115.

[56] Barkar I. et al., Optimization of elastic properties and weaving patterns of woven composites, Composite Structures 100 (2013) 575-591.

[57] Balaguru P., Nanni A. and Giancaspro, J., FRP composites for reinforced and prestressed concrete structures: A guide to fundamentals and design for repair and retrofit, Taylor & Francis (2009).

[58] Jaehyun K. et al., Mechanical properties of woven laminates and felt composites using carbon fibers, Part 1: in-plane properties, Composite Science and Technology 64 (2004) 2221-2229.

[59] Adams, R.D., et al., Stress analysis and failure properties of carbon-fibre-reinforced-plastic/steel double-lap joints, The Journal of Adhesion 20(1) (1986) 29-53.

[60] Park S. J., Effect of fiber-polymer interactions on fracture toughness behavior of carbon fiber-reinforced epoxy matrix composites, J Colloid Interface Sci 228 (2000) 287-291.

[61] Fu S. -Y et al., Tensile properties of short-glass-fiber- and short-carbon-fiber-reinforced polypropylene composites, Composites Part A 31 (2000) 1117-1125.

[62] Waltersson K., ESCA studies of carbon fibers: Part III-Surface reactions of carbon fibers with amines, Composite Sci Technol 23 (1985) 303-321.

[63] Tang L. G. and Kardos J. L., A review of methods for improving the interfacial adhesion between carbon fiber and polymer matrix, Polymer composites 18 (1997) 100-113.

[64] Mader E. et al., Static and dynamic properties of single and multi-fiber/epoxy composites modified by sizings, Composite science and technology 67 (2007) 1105-1115.

[65] Kowbel W., Bruce C. and Withers J. C., Effect of carbon fabric whiskerization on mechanical properties of C-C composites, Composite Part A 28 (1997) 993-1000.

[66] Tehrani M et al., Hybrid carbon fiber/carbon nanotube composites for structural damping applications, Nanotechnology 24 (2013) 155704.

[67] Skandani A. A. et al., Enhanced vibration damping of carbon fibers-ZnO nanorods hybrid composites, Applied Physics Letters 101 (2012) 073111.

[68] Paipetis A. and Galiotis C., A study of the stress-transfer characteristics in model composites as a function of material processing, fibre sizing and temperature of the environment, Composite Sci Technol 57 (1997) 827-838.

[69] Fu P. F., Luan Y., and Dai X. G., Interposition fixing structure of TiO_2 film deposited on activated carbon fibers, Transactions of nonferrous metals society of china 16 (2006) 965-969.

[70] Gaon J. C. and Prosen S. P., Interfacial bonding in graphite fiber-resin composites, American Society for Testing and Materials STP 452 (1969) 3-26.

[71] Zhang Q. et al., Hierarchical composites of carbon nanotubes on carbon fiber: influence of growth condition on fiber tensile propertie, Composites Sci Technol 69 (2009) 594-601.

[72] Rabenau A., The role of hydrothermal synthesis in preparative chemistry, Angew. Chem. 24 (1985) 1026-1040.

[73] Lin Y., Increased interface strength in carbon fiber composite through a ZnO nanowire interphase, Advanced functional materials 19 (2009) 2654-2660.

[74] Galan U., Effect of ZnO nanowire morphology on the interfacial strength of nanowire coated carbon fibers, Composite Sci Technol 71 (2011) 946-954.

[75] Lou X. W. et al., Template-free synthesis of SnO_2 hollow nanostructures with high lithium storage capacity, Adv. Mater 18 (17) (2006) 2325-2329.

[76] Gibson R. F., A review of recent research on mechanics of multifunctional composite materials and structures, Composite Struct 92 (2010) 2793-2810.

[77] Christodoulou L. and Venables J. D., Multifunctional material systems: the first generation, JOM 55 (2003) 39-45.

[78] Asp LE and Greenhalgh ES, Structural power composites, Compos Sci Technol 101 (2014) 41-61.

[79] Wang X. L. et al., Gel-based composite polymer electrolytes with novel hierarchical mesoporous silica network for lithium batteries, Electrochim Acta 53 (2008) 8001-8007.

[80] Croce F. et al., Nanocomposite polymer electrolyte for lithium batteries, Nature 394 (1998) 456-458.

[81] Gupta R. K. and Whang C. M., Structural study of a sol-gel derived novel solid oxide fuel cell perovskite, J Phys: Condens Matter 19 (2007) 196209.

[82] S. Arvinder and C. Amreesh, Significant Performance Enhancement in Asymmetric Supercapacitors based on Metal Oxides, Carbon nanotubes and Neutral Aqueous Electrolyte, Scientific Reports 5 (2015) 15551.

[83] Gonzalez A. et al., Review on supercapacitors: Technologies and materials, Renewable and Sustainable Energy Reviews 58 (2016) 1189-1206.

[84] M. Endo et al., High power electric double layer capacitor (EDLC's); from operating principle to pore size control in advanced activated carbons, Carbon Sci 1(3) (2001) 117-28.

[85] Zhang L. L. and Zhao X. S., Carbon-based materials as supercapacitor electrodes, Chem Soc Rev 38(9) (2009) 2520-2531.

[86] Wan J., Kang F. and Wei B., Engineering of MnO2-based nanocomposites for high-performance supercapacitors, Progress in Materials Science 74 (2015) 51-124.

[87] Kotz R. and Carlen M., Principles and applications of electrochemical capacitors, Electrochemica Acta 45 (1999) 2483-2498.

[88] Henson W., Optimal battery/ultracapacitor storage combination, J. Power Sources 179 (2008) 417-423.

[89] Wang H. and Pilon L., Physical interpretation of cyclic voltammetry for measuring electric double layer capacitance, Electrochimica Acta 64 (2012) 130-139.

[90] Karunya A., Rose C. and Nachiyar V., Biodegradation of the textile dye Mordant Black 17 (Calcon) by Moraxella osloensis isolated from textile effluent-contaminated site, World J Microbiol Biotechnol 30 (2014) 915-924.

[91] Frackowiak E. et al., Supercapacitors based on conducting polymer/nanotubes composites, Journal of Power Sources 153 (2006) 413-418.

[92] Winter M. et al., What are batteries, fuel cells, and supercapacitors?, American Chemical society 104 (2004) 4245-4269.

[93] Conway B. E., Double-layer and pseudo capacitance types of electrochemical capacitors and their applications to the development of hybrid devices, J Solid State Electrochem 7 (2003) 637-644.

[94] Conway B. E. et al., The role and utilization of pseudocapacitance for energy storage by supercapacitors, Journal of Power Sources 66 (1997) 1-14.

[95] Kong K., Kwon OB, Park HW, Enhanced mechanical and thermal properties of hybrid SnO2-woven carbon fiber composites using the facile controlled growth method, Composite Science and Technology 133 (2016) 60-69.

[96] Supothina S. et al., Effect of synthesis condition on morphology and yield of hydrothermal grown SnO_2 nanorod clusters, Journal of the European Ceramic Society 31 (2011) 2453-2458.

[97] Slater B. et al., Study of surface segregation of antimony on SnO_2 surfaces by computer simulation techniques, J. Phys. Chem. B 103 (48) (1999) 10644-10650.

[98] Leite E. R. et al., Crystal growth in colloidal tin oxide nanocrystals induced by coalescence at room temperature, Appl. Phys. Lett. 83 (8) (2003) 1566-1568.

[99] Pal U., Pal M. and Zeferino R. S., Gram-scale synthesis of highly crystalline, 0-D and 1-D SnO_2 nanostructures through surfactant-free hydrothermal process, J. Nanopart Res. 14(7) (2012) 969.

[100] Lupan O. et al., Synthesis of one dimensional SnO2 nanorods via a hydrothermal technique, Phys. E 41 (4) (2009) 533-536.

[101] Chen Y. J. et al., Synthesis and ethanol sensing characteristics of single crystaline SnO_2 nanorods, Appl. Phys. Lett. 87 (2005) 233503.

[102] Luo L. et al., Gas sensing characteristics of novel twin-layered SnO2 nanoarray fabricated by substratefree hydrothermal route, Sens. Actuat B-Chem. 218 (2015) 205-214.

[103] Zou R. et al., Heterostructures of Vertical, Aligned and Dense SnO2 nanorods on Graphene sheets: in-situ TEM measured mechanical, electrical and field emission properties, J. Mater. Chem. 22 (2012) 19196

[104] Mi H. Y. et al., Silver nanowire/thermoplastic polyurethane elastomer nanocomposites: thermal, mechanical, and dielectric properties, Mater Des. 56 (2014) 398-404.

[105] Russo P. et al., Tensile properties, thermal and morphological analysis of thermoplastic polyurethane films reinforced with multiwalled carbon nanotubes, European Polymer Journal 49 (2013) 3155-3164.

[106] Xie X. Q. et al., A comparative investigation on the effects of nitrogen-doping into graphene on enhancing the electrochemical performance of SnO_2/graphene for sodium-ion batteries, Nanoscale 7 (2015) 3164-3172.

[107] Jiang Y. et al., Enhancing the cycling stability of Na-ion batteries by bonding SnS_2 ultrafine nanocrystals on amino functionalized graphene hybrid nanosheets, Energy Environ. Sci. 9 (2016) 1430-1438.

[108] Javid A. et al., Carbon fibre-reinforced poly(ethylene glycol) diglycidylether based multifunctional structural supercapacitor composites for electrical energy storage applications, Journal of composite materials 50 (2016) 2155-2163.

[109] Shirshova N. et al., Polymerised high internal phase ionic liquid-in-oil emulsions as potential separators for lithium ion batteries, J. Mater. Chem. A 1 (2013) 9612-9619.

[110] Shirshova N. et al., Structural supercapacitor electrolytes based on bicontinuous ionic liquid-epoxy resin systems, J. Mater. Chem. A 1 (2013) 15300-15309.

[111] Wali Q. et al., One pot synthesis of multi-functional tin oxide nanostructures for high efficiency dye-sensitized solar cells, Journal of Alloys and Compounds 646 (2015) 32–39.

[112] Yadav A. A., SnO_2 thin film electrodes deposited by spray pyrolysis for electrochemical supercapacitor applications, J Mater Sci: Mater Electron 27 (2016) 1866-1872.

[113] Zheng H. M. et al., TiO_2@C core-shell nanowires for high-performance and flexible solid-state supercapacitors, J. Mater. Chem. C 1 (2013) 225–229.

[114] Gu L. et al., Performance Characteristics of Supercapacitor Electrodes Made of Silicon Carbide Nanowires Grown on Carbon Fabric, J. Power Sources 243 (2013) 648–653.

[115] Lu X. H. et al., Hydrogenated TiO_2 Nanotube Arrays for Supercapacitors, Nano Lett. 12 (2012) 1690-1696.

[116] Bae J. et al., Fiber Supercapacitors Made of Nanowire-Fiber Hybrid Structures for Wearable/Flexible Energy Storage, Angew. Chem. Int. Ed. 50 (2011) 1683-1687.

[117] Fletcher S., Black V. J. and Kirkpatrick I., A universal equivalent circuit for carbon based supercapacitors, J Solid State Electrochem 18 (2014) 1377-1387.

[118] Senthilkumar S. T. et al., Electric double layer capacitor and its improved specific capacitance using redox additive electrolyte, J. Mater. Chem. A 1 (2013) 1086-1095.

[119] Chen T. and Dai L., Flexible supercapacitors based on carbon nanomaterials, J. Mater. Chem. A 2 (2014) 10756-10775.

[120] Portet C. et al., Capacitance of KOH activated carbide-derived carbons, Phys. Chem. Chem. Phys. 11 (2009) 4943-4945.

[121] Greenhalgh E. S. et al., Mechanical, electrical and microstructural characterisation of multifunctional structural power composites, J Compos Mater 49 (2015) 1823–1834.

[122] Maxwell BCAP0010 datasheet, www.maxwell.com/products/ultracapacitors/docs/datasheet_hc_ series_ 1013793.pdf (2014).

[123] Liu C. et al., Graphene-based supercapacitor with an ultrahigh energy density, Nano Lett. 10 (2010) 4863-4868.

[124] Bae J. et al., Toward wearable and stretchable fabric-based supercapacitors: novel ZnO and SnO_2 nanowires-carbon fibre and carbon paper hybrid structure, J Solid State Electrochem 19 (2015) 211-219.

[125] Yanping Z. et al., Carbon nanotube-zinc oxide electrode and gel polymer electrolyte for electrochemical supercapacitors, Journal of Alloys and Compounds 480 (2009) L17-L19.

[126] Jayalakshmi M. et al., Single step solution combustion synthesis of ZnO/carbon composite and its electrochemical characterization for supercapacitor application, Int. J. Electrochem. Sci. 3 (2008) 96-103.

[127] Ming-Jay D. et al., Facile electrochemical synthesis of 3D nano-architectured CuO electrodes for high-performance supercapacitors, J. Mater. Chem. A 2 (2014) 12857-12865.

[128] Hongxia Z., Jing F. and Milin Z., Preparation of flower-like CuO by a simple chemical precipitation method and their application as electrode materials for capacitor, Materials Rerearch Bulletin 43 (2008) 3221-3226.

[129] Yu Z. X. et al., Controlled synthesis of hierarchical CuO nanostructures for electrochemical capacitor electrodes, Int. J. Electrochem. Sci. 8 (2013) 8645-8661.

7. Acknowledgement

First of all, I would like to express my sincerest thanks and appreciation to my advisor Professor Dr. Hyung Wook Park. Without his kind and patient guidance and knowledge, this study would never been completed. His zest and keen knowledge about work continuously gave me motivations for this study. I am honored that I could study under Dr. Hyung Wook Park.

I would like to express my sincere gratitude to committee members, Dr. Young Bin Park, Dr. Han Gi Chae. It would be difficult to finish the study without their beneficent advice.

I extremely grateful to lab members in Multi-scale Hybrid Manufacturing Laboratory; Dr. Deka, Dr.Ankita, Kyoung Il Kong, Dong Min Kim, Ji Su Kim, Jae Woo Seo, Do Young Kim, Young Bin Kim, Minji Kim and Wu Jin Lee for their support.

Especially, I would like to thank Dr. Deka and Dr. Ankita. They gave me lots of advices and helps for my study. With their warm kindness I could finish my work successfully.

I would express a deep sense of gratitude to my family for their unstinting support and limitless trust. I would not be here without my precious family. My parents are my only one role model and I will be the proud son.

Last but not least, I would also thank to people who were not mentioned here.

Thanks.